

Probing B-Anomalies via Dimuon Tails at a Future Collider

Bradley Garland¹, Sebastian Jäger¹, Charanjit K. Khosa^{2,3}, and Sandra Kvedaraitė^{*4}

¹Department of Physics and Astronomy, University of Sussex, Brighton BN1 9QH, UK.

²H.H. Wills Physics Laboratory, University of Bristol, Tyndall Avenue, Bristol BS8 1TL, UK.

³Dipartimento di Fisica, Università di Genova and INFN, Sezione di Genova, Via Dodecaneso 33, 16146, Italy.

⁴Department of Physics, University of Cincinnati, Cincinnati, OH 45221, USA.

Abstract

We investigate the sensitivity of future proton-proton colliders to a contact interaction of the form $1/\Lambda^2 (\bar{b}_L \gamma_\mu s_L) (\bar{\mu}_L \gamma^\mu \mu_L)$ as indicated by the long-standing rare B -decay anomalies. We include NLO QCD and electroweak effects and employ an optimized binning scheme, and carefully validate our background calculation against ATLAS and CMS data. We find that the FCC-hh with 40 ab^{-1} of luminosity is able to exclude scales Λ up to 26 TeV at 95% CL, and discover Λ up to 20 TeV. While this is not quite enough to exclude or discover the current best-fit value of 39 TeV, this can in principle be achieved with more luminosity and/or higher energy, as we study quantitatively. Our analysis is conservative in that it assumes *only* a $\bar{b}s\mu\mu$ contact interaction.

1 Introduction

In recent years, a number of measurements of rare semileptonic $b \rightarrow s \ell^+ \ell^-$ transitions have shown significant discrepancies with Standard Model (SM) predictions (see [1, 2] for reviews). A particularly clear picture is provided by measurements of the lepton-flavour-universality (LFU) ratios [3]

$$R_{K^{(*)}} = \frac{\text{BR}(B \rightarrow K^{(*)} \bar{\mu} \mu)}{\text{BR}(B \rightarrow K^{(*)} \bar{e} e)}, \quad (1.1)$$

together with the purely leptonic branching fraction $\text{BR}(B_s \rightarrow \mu^+ \mu^-)$, for which theoretical uncertainties are currently negligible compared to experimental statistical ones (Table 1). This “clean” dataset on its own is currently at variance with the SM at 4.2σ significance ([4], October 2021 update). It is the goal of this paper to study the implications of the rare B decay anomalies for future pp colliders, in a manner as model-independent and conservative as possible. We will be focusing on the inclusive dimuon signal $pp \rightarrow \mu^+ \mu^-$. The rare B -decay data can be model-independently described by new beyond-SM (BSM) four-fermion contact interactions in the low-energy effective weak Hamiltonian involving muons only,

$$\begin{aligned} \mathcal{L}_{\text{eff}}^{\text{BSM}} = -\mathcal{H}_{\text{eff}}^{\text{BSM}} &= \frac{4G_F}{\sqrt{2}} V_{ts} V_{tb}^* \frac{e^2}{16\pi^2} \{ C_9^{\text{NP}} (\bar{b}_L \gamma_\mu s_L) (\bar{\mu} \gamma^\mu \mu) + C_{10}^{\text{NP}} (\bar{b}_L \gamma_\mu s_L) (\bar{\mu} \gamma^\mu \gamma^5 \mu) + \dots \} \\ &\equiv \frac{1}{\Lambda_{\text{LL}}^2} (\bar{b}_L \gamma_\mu s_L) (\bar{\mu}_L \gamma^\mu \mu_L) + \frac{1}{\Lambda_{\text{LR}}^2} (\bar{b}_L \gamma_\mu s_L) (\bar{\mu}_R \gamma^\mu \mu_R) + \dots \end{aligned} \quad (1.2)$$

*Email: b.garland@sussex.ac.uk, s.jaeger@sussex.ac.uk, charanjit.kaur@bristol.ac.uk, kvedarsa@ucmail.uc.edu

Observable	SM	Measurement	Experiment
$BR(B_s \rightarrow \mu^+ \mu^-)$	$(3.63 \pm 0.13) \times 10^{-9}$	$(2.8 \pm 0.3) \cdot 10^{-9}$	average [4] of ATLAS [5], CMS [6] and LHCb [7]
$R_K[1.1, 6]$	$1.0004^{+0.0008}_{-0.0007}$	0.85 ± 0.04	LHCb [8]
$R_K[1, 6]$		1.03 ± 0.28	Belle [9]
$R_{K^*}[0.045, 1.1]$	$0.920^{+0.007}_{-0.006}$	0.66 ± 0.11	LHCb [10]
		0.52 ± 0.37	Belle [11]
$R_{K^*}[1.1, 6]$	0.996 ± 0.002	0.69 ± 0.12	LHCb [10]
		0.96 ± 0.45	Belle [11]

Table 1: Selection of $b \rightarrow s\ell^+\ell^-$ data. The notation $R_{K^{(*)}}[a, b]$ refers to a dilepton mass bin $a \text{ GeV}^2 < q^2 < b \text{ GeV}^2$. Theory predictions for $R_K^{(*)}$ are taken from [12] and for $BR(B_s \rightarrow \mu^+\mu^-)$ from [13]. Predictions for $R_{K^{(*)}}$ do not include effects of electromagnetic radiation. These are on the order of a few percent, and corrected for by experiments, with the residual error currently negligible compared to experimental statistical uncertainties [14, 15].

In Eq. 1.3 the ellipses refer to additional operators with different Dirac structures which are not favoured by the data. In fact, an excellent description of all $b \rightarrow s\ell^+\ell^-$ data is obtained by a purely left-handed interaction, $C_9^{\text{NP}} = -C_{10}^{\text{NP}} \equiv C_L$ [4, 16, 17]. In [4], a fit to the “clean” data alone resulted in the 1σ range $C_L = -0.40^{+0.09}_{-0.08}$; a fit also including angular data in $B \rightarrow K^*\ell^+\ell^-$ gave a very similar value $C_L = -0.39^{+0.08}_{-0.09}$. Fitting the global dataset jointly to C_9 and C_{10} and profiling over the combination $C_R = (C_9 + C_{10})/2$ gave instead $C_L = -0.43^{+0.10}_{-0.10}$. Refs. [16, 17] find very similar C_L ranges. In other words, the value of C_L is well determined and rather robust against the choice of dataset and whether a coupling to right-handed muons is allowed or not. In summary, the rare B decay dataset points to the presence of a left-handed contact interaction

$$\mathcal{L}_{\text{eff}} \supset \frac{1}{\Lambda^2} \mathcal{O}_{LL}, \quad (1.3)$$

where $\mathcal{O}_{LL} = (\bar{b}_L \gamma_\mu s_L) (\bar{\mu}_L \gamma^\mu \mu_L)$ and

$$\Lambda = (39 \pm 4) \text{TeV}, \quad (1.4)$$

and allows for the possible presence of an additional coupling to right-handed muons.

The interaction Eq. 1.3 provides a minimal description of all rare B -decay anomalies and in the following we will assume it is the only BSM interaction present. While it is possible that further interactions are present in the effective Hamiltonian, they do not improve the description of the data further [17, 18]. Importantly, they will tend to increase the signal in $pp \rightarrow \mu^+\mu^-$ further, either because the C_L value in the fit remains the same or because a comparable or larger Wilson coefficient appears instead. For example, a model employing operators with electrons instead of muons still fits the data significantly better than the SM (though not as well as Eq. 1.3, as it does not contribute to the $B \rightarrow K^*\mu^+\mu^-$ angular observables, $B_s \rightarrow \mu^+\mu^-$, etc.). In addition, the fitted interaction strength is close in magnitude to the muonic case considered here [16, 18] and would generate a comparable $pp \rightarrow e^+e^-$ signal at a collider. Altogether, our assumption of a minimal interaction Eq. 1.3 is a conservative one, in that it will lead to conservative results for the sensitivity at a future collider.

The minimal effective interaction Eq. 1.3 can be interpreted as a low-energy effective description of an extension of the SM by new degrees of freedom. A plethora of such simplified

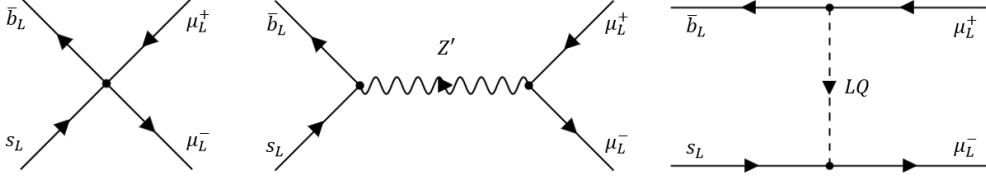


Figure 1: Feynman diagrams for a purely left-handed effective $bs\mu\mu$ operator (left) and the two possible tree-level mediators of contact interactions of this type; Z' (middle) and leptoquark (right).

models and possible UV completions has been constructed. The simplest and most studied involve tree-level exchange of a neutral vector (Z') or a (spin-1 or spin-0) leptoquark (see Fig. 1). Such mediators can be directly searched for at the LHC. For example, a Z' mediator would cause a bump in the inclusive dimuon signal [19, 20]. The sensitivity of the LHC and future colliders to tree-level mediators that can underpin the rare B -decay anomalies has been studied for the Z' case in [21, 22, 23, 24] and for leptoquarks in [25, 26, 27] (see also [28, 29]); for the collider signatures of other models of the B -physics anomalies see [1, 2] and references therein. Such searches are necessarily model-dependent, and, even at a 100 TeV machine, do not cover the entire parameter space. For example, the mediator could simply be too heavy: perturbative unitarity alone would allow, for $\Lambda = 39$ TeV, mediators as heavy as 105 TeV [30].

Another, more model-independent approach is to look for the effects of heavy new physics in the “low-energy” tails of the dilepton invariant mass and other distributions within the context of effective field theory [31, 32]. Ref. [31] employed the ATLAS inclusive dimuon search [33] to obtain a 95% confidence level (CL) bound of $\Lambda > 2.5$ TeV, and a projected bound of $\Lambda > 4.1$ TeV at the HL-LHC for $L = 3000 \text{ fb}^{-1}$ at $\sqrt{s} = 13$ TeV. Ref. [34] (see also [35]) investigated final states including a dimuon and a b -jet, obtaining a projected bound $\Lambda > 7.7$ TeV for $L = 3000 \text{ fb}^{-1}$ at $\sqrt{s} = 13$ TeV. More recent LHC dimuon searches and the ATLAS search have been published in [33, 36, 37]. Ref. [38] considered the prospects at a muon collider, with encouraging results.

With the LHC and HL-LHC falling short of being able to detect Eq. 1.3 for $\Lambda \sim 40$ TeV, the question is, to what extent does increased collider centre of mass (c.o.m) energy \sqrt{s} improve the sensitivity to $bs\mu\mu$ contact interactions? In the present paper, we investigate this using the tails of the inclusive dimuon invariant mass $m_{\bar{\mu}\mu}$ distributions. We take the proposed $\sqrt{s} = 100$ TeV FCC-hh as a baseline whilst also providing updated limits at the $\sqrt{s} = 14$ TeV HL-LHC. We derive both 95% CL exclusion limits and expected 5σ discovery sensitivities. In doing so, we include the NLO QCD and EW corrections to our EFT signal. We also consider the validity of our limits from the perspective of partial-wave unitarity and the EFT expansion.

The remainder of this paper is organised as follows. In Sec. 2 we describe our basis and notations for the $bs\mu\mu$ contact interaction within the SMEFT framework. Sec. 3 is devoted to our analysis set-up where we discuss event simulation, statistical methods, event selection as well as commenting on unitarity constraints and the validity of EFT approach. Our findings are detailed in Sec. 4 where we give limits at $\sqrt{s} = 14$ TeV, $\sqrt{s} = 100$ TeV and beyond. We conclude in Sec. 5.

2 Standard Model Effective Field Theory

At energies above the electroweak scale, but below the mass scale of the underlying UV physics, the interaction Eq. 1.3 is appropriately described within the framework of the SMEFT. The SMEFT Lagrangian is an expansion in local operators of increasing mass dimension,

$$\mathcal{L}^{\text{SMEFT}} = \mathcal{L}^{\text{SM}} + \sum_i c_i^{(6)} \mathcal{O}_i^{(6)} + \sum_j c_j^{(8)} \mathcal{O}_j^{(8)} + \dots \quad (2.1)$$

constructed out of the SM fields, where $\mathcal{O}_i^{(D)}$ is a gauge invariant operator of dimension D and $c_i^{(D)}$ is its corresponding Wilson coefficient. For later convenience, we note that the Wilson coefficients $c_i^{(D)}$ can be expressed as the ratio of a dimensionless coupling $g_i^{(D)}$ and an arbitrary mass scale $\hat{\Lambda}$ such that

$$c_i^{(D)} = \frac{g_i^{(D)}}{\hat{\Lambda}^{D-4}}. \quad (2.2)$$

The predictivity of the SMEFT rests on the higher-dimensional operators in Eq. 2.1 being suppressed such that the expansion can be truncated at some dimension such that the remainder can be neglected; in our work we will truncate at the leading BSM dimension 6. A separate requirement is that the truncated amplitude satisfies S -matrix unitarity constraints. These questions will be discussed in more detail in Sec. 3.4.

The relevant dimension-6 gauge invariant operators that contribute to purely left-handed four-fermion interactions can be found in [39, 40]. Ignoring flavour indices, there are two dimension-6 semileptonic operators with a $(\bar{\mathbf{L}}\mathbf{L})(\bar{\mathbf{L}}\mathbf{L})$ chirality structure. In the Warsaw basis [40], and including flavour indices, we have

$$\begin{aligned} \mathcal{L}^{\text{SMEFT}} &\supset \frac{c_{QijL\mu\mu}^{(3)}}{\hat{\Lambda}^2} (\bar{Q}_j \gamma_\rho \sigma^a Q_i) (\bar{L}_2 \gamma^\rho \sigma_a L_2) + \frac{c_{QijL\mu\mu}^{(1)}}{\hat{\Lambda}^2} (\bar{Q}_j \gamma_\rho Q_i) (\bar{L}_2 \gamma^\rho L_2) \\ &\equiv \frac{c_{QijL\mu\mu}^{(3)}}{\hat{\Lambda}^2} \mathcal{O}_{ij}^{(3)} + \frac{c_{QijL\mu\mu}^{(1)}}{\hat{\Lambda}^2} \mathcal{O}_{ij}^{(1)}, \end{aligned} \quad (2.3)$$

where i, j run over the generations of quarks and leptons, $Q_i = (V_{ji}^* u_L^j, d_L^i)^T$, $L_i = (\nu_L^i, l_L^i)^T$ and σ^a are the Pauli matrices.

It is convenient to express Eq. 2.3 in a different operator basis,

$$\mathcal{O}_{ij}^\pm = \frac{1}{2} \left(\mathcal{O}_{ij}^{(1)} \pm \mathcal{O}_{ij}^{(3)} \right), \quad C_{ij}^\pm = \frac{c_{QijL\mu\mu}^{(1)} \pm c_{QijL\mu\mu}^{(3)}}{\hat{\Lambda}^2}, \quad (2.4)$$

such that

$$\begin{aligned} \mathcal{L}^{\text{SMEFT}} &\supset C_{ij}^+ (\bar{d}_L^j \gamma_\rho d_L^i) (\bar{\mu}_L \gamma^\rho \mu_L) + C_{ij}^- (\bar{d}_L^j \gamma_\rho d_L^i) (\bar{\nu}_\mu \gamma^\rho \nu_\mu) + \\ &\quad \sum_{k,l} V_{ki}^* C_{ij}^+ V_{lj} (\bar{u}_L^l \gamma_\rho u_L^k) (\bar{\nu}_\mu \gamma^\rho \nu_\mu) + \sum_{k,l} V_{ki}^* C_{ij}^- V_{lj} (\bar{u}_L^l \gamma_\rho u_L^k) (\bar{\mu}_L \gamma^\rho \mu_L). \end{aligned} \quad (2.5)$$

The benefit of working in the (C_{ij}^+, C_{ij}^-) basis is that the \mathcal{O}^+ operators couple muons to down-type quarks only, and the \mathcal{O}^- operators to up-type quarks only. In particular, the $b \rightarrow s \mu^+ \mu^-$ transitions are governed by a single Wilson coefficient C_{sb}^+ .

In the present paper, we consider the minimal scenario in which our EFT signal is given by Eq. 1.3, which in the SMEFT corresponds to

$$C^+ = \begin{pmatrix} 0 & 0 & 0 \\ 0 & 0 & C_{sb}^+ \\ 0 & C_{sb}^{+*} & 0 \end{pmatrix} \quad C^- = \begin{pmatrix} 0 & 0 & 0 \\ 0 & 0 & 0 \\ 0 & 0 & 0 \end{pmatrix}. \quad (2.6)$$

We then have

$$\mathcal{L}^{\text{SMEFT}} \supset C_{sb}^+ (\bar{b}_L \gamma_\rho s_L) (\bar{\mu}_L \gamma^\rho \mu_L) + \sum_{k,l} V_{ks}^* C_{sb}^+ V_{lb} (\bar{u}_L^l \gamma_\rho u_L^k) (\bar{\nu}_\mu \gamma^\rho \nu_\mu) + \text{h.c.}, \quad (2.7)$$

and by comparing to Eq. 1.3 we have

$$C_{sb}^+ = \frac{1}{\Lambda^2}. \quad (2.8)$$

We stress that this is a conservative assumption: in a UV model, there will typically be additional nonzero entries in the matrices C^+ and C^- , such as for example a $\bar{b}b\bar{\mu}\mu$ coupling. In the $pp \rightarrow \mu^+\mu^-$ process we will consider, such additional couplings will generate additional contributions to the signal, enhancing the sensitivity to the interaction. The signal we will consider is the minimal one required by the rare B -decay anomalies, and therefore the exclusion and discovery reach we will find are conservative and universally applicable, subject only to EFT validity/applicability requirements.

3 Analysis Set-up

In this section we describe the set-up of our analysis. We start by discussing the methods used to obtain the contributions of the SM background and EFT signal to the dimuon invariant mass $m_{\bar{\mu}\mu}$ spectrum. We then describe the statistical methods used to assess the sensitivity of a future collider with c.m. energy \sqrt{s} to the EFT signal. In our analysis, we are principally concerned with the $\sqrt{s} = 14$ TeV HL-LHC and the proposed $\sqrt{s} = 100$ TeV FCC-hh. Finally, we detail the event selection and binning schemes used at different c.o.m energies before discussing the constraints on our sensitivity calculations arising from tree-level unitarity and the validity of the EFT expansion.

3.1 Event Simulation

In this subsection we detail how we obtain the dimuon invariant mass $m_{\bar{\mu}\mu}$ distributions used in our sensitivity calculations. We first describe how we model the SM background, validating our modeling of the SM background by comparing it to the latest ATLAS [41] and CMS [36] searches for non-resonant phenomena in high-mass dilepton final states at $\sqrt{s} = 13$ TeV. This validation allows us to proceed with obtaining the background at the future collider. We then discuss the modeling of the EFT signal where we include the next to leading order effects in both the QCD and EW couplings.

The relevant SM processes that contribute to $pp \rightarrow \mu^+\mu^-$ are Drell–Yan (DY) via Z/γ^* exchange, diboson (ZZ , WZ and WW) production and top-quark production ($t\bar{t}$ & tW). The dominant contribution is DY which, at $\sqrt{s} = 13$ TeV, makes up $\sim 80\%$ of all events in the region where $m_{\bar{\mu}\mu} > 600$ GeV and $\sim 90\%$ in the region where $m_{\bar{\mu}\mu} > 1300$ GeV. To model the DY process we use MADGRAPH5_AMC@NLO [42, 43]. Specifically, we perform combined NLO QCD and EW fixed order calculations to obtain the cross section of the DY process in chosen

bins in the dimuon invariant mass. To model the top quark and diboson background we again use MADGRAPH5_AMC@NLO. However, since these effects are subleading, we only consider the LO contributions.

Our calculations are performed using the NNPDF31_NLO_AS_0118_LUXQED PDF set [44] via LHAPDF6 [45] in the 5 flavour scheme¹. In regards to the EW calculations to the EFT signal and Drell-Yan process, we use the G_μ -scheme as an input scheme. We also consider dressed muons in the final state. Here collinear muon-photon pairs arising from real photon emission are recombined if they lie within a cone of radius $R_{\text{rec}} = 0.1$ around the muon. This ensures IR insensitivity and reliability of fixed-order results.

The number of events in a given bin N_{bin} of the invariant mass distribution is calculated using

$$N_{\text{bin}} = \varepsilon^2 L \sigma_{\text{bin}}. \quad (3.1)$$

Here σ_{bin} is the cross section of the given process in a given bin (this applies to the EFT signal also), L is the total integrated luminosity and ε is the combined muon identification and reconstruction efficiency of the given pp -collider considered. A detector's ability to identify and reconstruct muons produced in collisions can significantly affect our sensitivity calculations and such detector effects are especially important when comparing to experimental analyses. We address the problem of muon identification and reconstruction by introducing ε in Eq. 3.1. When comparing to experimental analysis at $\sqrt{s} = 13$ TeV or performing sensitivity calculations at the $\sqrt{s} = 14$ TeV HL-LHC, we take $\varepsilon = 0.75$ ($\varepsilon = 0.965$) for the ATLAS [19, 46] (CMS [36]) detector. For a future collider with $\sqrt{s} = 100$ TeV we use a muon identification efficiency $\varepsilon = 0.95$ in line with Ref. [47].

Due to the inclusiveness of the dimuon final state, the need to conduct a full Monte-Carlo collider simulation with parton shower is largely unnecessary. In Fig. 2, it can be seen that our SM background is in excellent agreement with the latest ATLAS and CMS searches. To generate the distributions shown in Fig. 2 we apply the same cuts on the transverse momentum p_T and pseudo-rapidity η of the muons as done in the ATLAS [41] and CMS analyses [36]. When comparing to the ATLAS search, we use $p_T > 30$ GeV and $|\eta| < 2.5$ and, for the CMS search, we use $p_T > 53$ GeV and $|\eta| < 2.4$.

In Fig. 2 it can be seen that our SM background lies within $\sim 10\%$ of the CMS simulation. Our accuracy to the ATLAS simulation is slightly worse; however, this can be put down to the more complex selection criteria used in the ATLAS search and the method used to extract the data from Fig. 5 of the auxiliary material of [41]. Having validated our modeling of SM backgrounds at $\sqrt{s} = 13$ TeV we can use this to obtain a good estimate of the SM background at a $\sqrt{s} = 100$ TeV collider. The invariant mass of dimuon pairs originating from the SM background at $\sqrt{s} = 100$ TeV is shown in Fig. 3 over the range $m_{\bar{\mu}\mu} = [2.5, 40]$ TeV.

Similarly to the SM background, MADGRAPH5_AMC@NLO is used to compute the EFT signal cross-section. We again perform combined NLO fixed order calculations including both the QCD and EW couplings. To this end, a UFO model [48] was created in which the dim-6 terms in Eq. 2.7 were added to the default SM UFO model used by MADGRAPH5_AMC@NLO. For NLO calculations of the EFT signal to yield physical gauge-invariant results, rational terms, specifically R_2 terms, must be added to the model file by hand. The necessary R_2 terms for the EFT signal have been calculated for the first time here and were thus included in the UFO model file used in this study. For more details on the calculation of the rational R_2 terms see Appendix A.

¹It is noted that we use the 4 flavour scheme when modeling the background arising from top quark production.

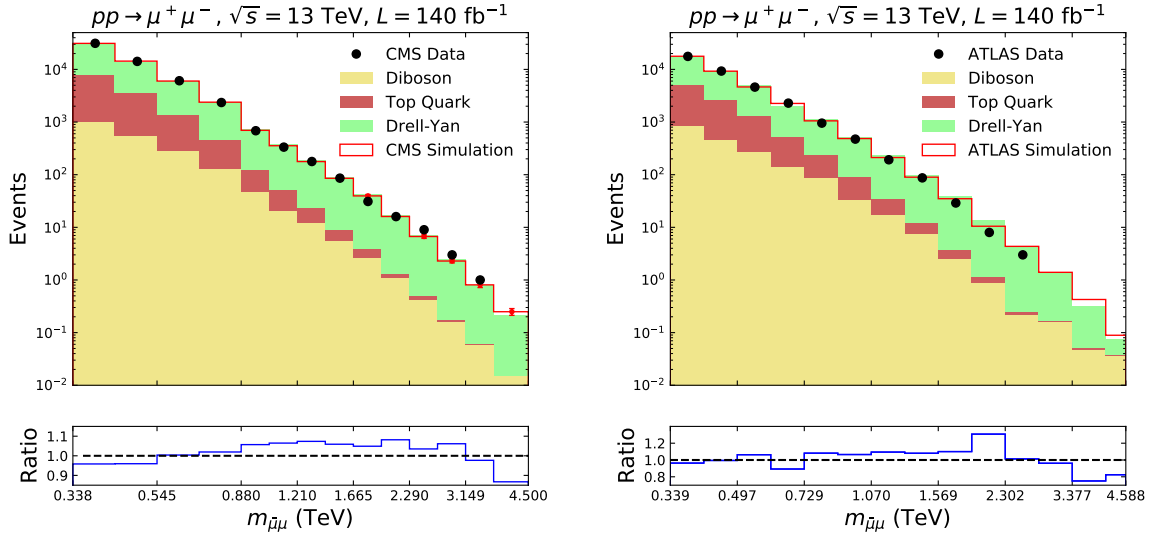


Figure 2: Comparison of our SM background, generated using the methodology outlined in Sec. 3.1, and the reported backgrounds and data from the recent CMS [36] (left) and ATLAS [41] (right) searches. The observed data and predicted background from Monte Carlo simulations are directly taken from Fig. 2 in [36] and Fig. 5 of the auxiliary material of [41]. In the left plot we have included the uncertainty in CMS background calculation. The lower panel of both plots gives the ratio of the number of events in each bin from our background calculation to the number calculated in the CMS or ATLAS simulations.

The motivation for including the NLO corrections to the EFT signal comes from the fact that the DY process receives large EW corrections in the high dilepton invariant mass region. Specifically, the NLO-EW corrections contain large negative Sudakov double logarithms that have been seen to reduce the differential cross section $d\sigma/dm_{\bar{\mu}\mu}$ of the inclusive DY process at large values of $m_{\bar{\mu}\mu}$. At $\sqrt{s} = 13$ TeV it is seen that the differential cross section reduces by more than 30% for values of $m_{\bar{\mu}\mu} > 1$ TeV [49]. The Sudakov double logarithms that cause such large negative corrections to the DY cross section originate from Feynman diagrams in which two external legs exchange a virtual particle. Given this, analogous NLO-EW diagrams exist for the EFT signal where the s-channel mediator is replaced by an effective vertex (see diagrams of Type A, B, and C in Appendix A).

In Fig. 4 we plot the ratio of the NLO cross section to the LO cross section as a function of a lower cut on $m_{\bar{\mu}\mu}$ for both the EFT signal and the DY process. Here, we consider three NLO to LO ratios with the NLO cross section corresponding to the pure NLO-QCD, pure NLO-EW or the combined NLO-QCD&EW cross section. In Fig. 4, it is seen that the inclusion of the pure NLO-QCD corrections yields a consistent $\sim 10\%$ increase in both the EFT signal and DY cross section at $\sqrt{s} = 13$ TeV and $\sqrt{s} = 100$ TeV. However, it is a different story for the NLO-EW corrections. For the DY process the NLO-EW corrections are seen to decrease the cross section by as much as $\sim 20\%$ at $\sqrt{s} = 13$ TeV and $\sim 45\%$ at $\sqrt{s} = 100$ TeV. Again, this is due to the presence of large negative Sudakov double logarithms. Whilst logarithms of this type reduce the NLO-EW EFT signal cross section, the effect is less dramatic than that seen for DY. In fact, the combined NLO-QCD&EW signal cross section is always within 10% of the LO cross section. Ultimately, this effect is not as large as may have been expected and a 10% variation in the signal cross section does not have a significant effect on our sensitivity calculations.

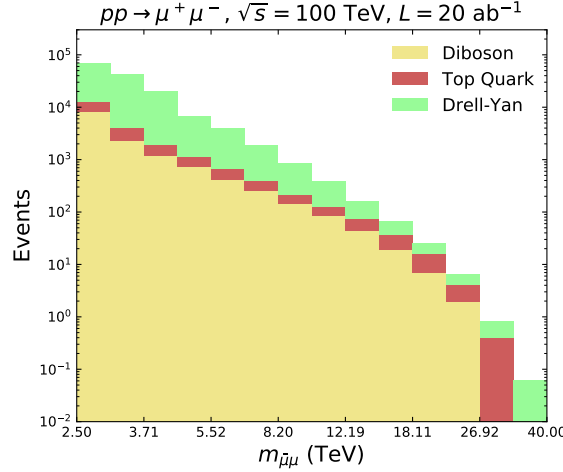


Figure 3: The Standard Model background at $\sqrt{s} = 100$ TeV calculated with a total integrated luminosity of $L = 20$ ab^{-1} and muon identification efficiency $\epsilon = 0.95$.

3.2 Statistics

Here we characterise the sensitivity of the HL-LHC and a future collider to the EFT signal detailed in Sec. 2. To do this we perform two types of statistical tests based on binned dimuon invariant mass distributions. Given a certain signal strength, characterised by the mass scale Λ in Eq. 2.8, we calculate the expected significance to reject a given null hypothesis H_0 in favour of an alternative hypothesis H_1 . Our statistical methods closely follow those developed and outlined in [50].

The first statistical test we perform involves setting exclusion limits on Λ . Here we define H_0 to be the signal+background hypothesis with H_1 being the background only hypothesis. We then derive the value of the Λ needed to reject the signal+background hypothesis at the 95% CL. Our second statistical test involves the discovery of the EFT signal. Here the roles of H_0 and H_1 are reversed and we calculate the value of Λ needed to reject the background only hypothesis at the $n\sigma$ level.

To calculate the expected significance, we construct a profile likelihood ratio from our binned invariant mass distributions. We first define a test statistic t_{μ} to measure the level of agreement between H_1 and H_0 . Our test statistic is given by

$$t_{\mu} = -2 \ln \lambda(\mu), \quad (3.2)$$

where $\lambda(\mu)$ is a profile likelihood ratio given by

$$\lambda(\mu) = \frac{L(\mu)}{L(\hat{\mu})}. \quad (3.3)$$

Here $\mu = (\mu_1, \mu_2, \dots, \mu_N)$, where μ_j parameterizes the strength of the signal process in the j^{th} bin. For a histogram with N bins, the likelihood function $\mathcal{L}(\mu)$ is constructed treating every bin as an independent Poisson variable such that

$$\mathcal{L}(\mu) = \prod_{j=1}^N \frac{(\mu_j s_j + b_j)^{n_j}}{n_j!} e^{-(\mu_j s_j + b_j)}. \quad (3.4)$$

Here, s_j and b_j are the expected number of signal and background events in the j^{th} bin respectively and n_j is the total number of events in the j^{th} bin according to the alternate hypothesis

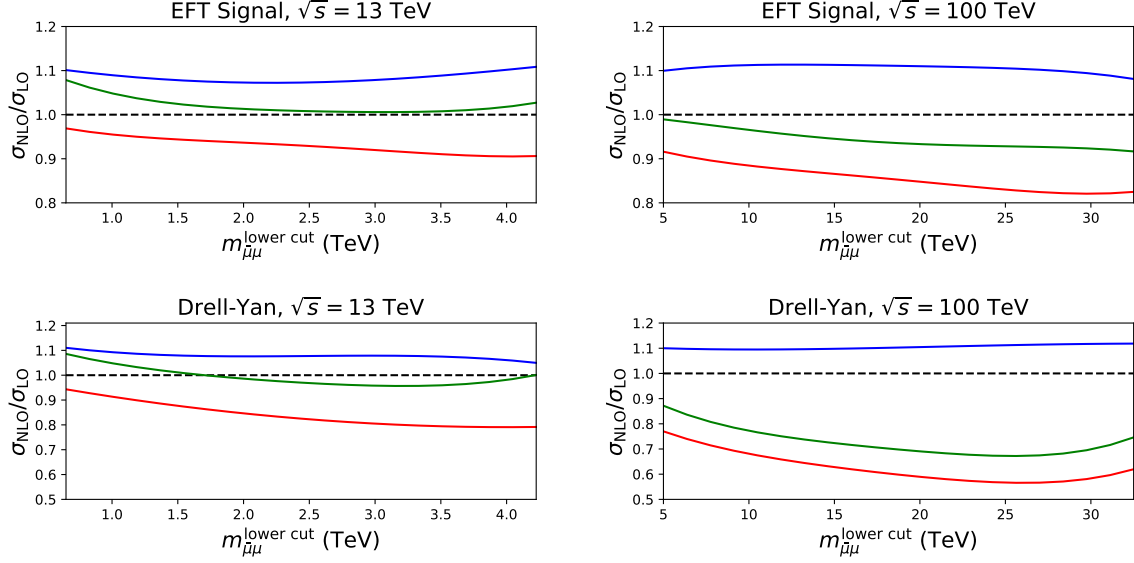


Figure 4: The ratios of the NLO-QCD, NLO-EW and NLO-QCD&EW cross sections to the LO cross section for both the EFT signal and the DY process as a function of a lower cut on the dimuon invariant mass $m_{\mu\mu}^{\text{lower cut}}$. The blue lines correspond to NLO-QCD, the red to NLO-EW and the green to NLO-QCD&EW. The following cuts on muons are used: at $\sqrt{s} = 13$ TeV, $p_T = 52$ GeV and $|\eta| < 2.5$ and at $\sqrt{s} = 100$ TeV, $p_T = 400$ GeV and $|\eta| < 4.0$.

H_1 . Finally, $\hat{\boldsymbol{\mu}} = (\hat{\mu}_1, \hat{\mu}_2, \dots, \hat{\mu}_N)$ is the maximum-likelihood estimator of $\boldsymbol{\mu}$ which, in this instance, is given by $\hat{\mu}_j = (n_j - b_j)/s_j$.

The significance to reject the null hypothesis is given by

$$Z_{\boldsymbol{\mu}} = \sqrt{t_{\boldsymbol{\mu}}}. \quad (3.5)$$

To calculate the expected significance $E[Z_{\boldsymbol{\mu}}]$ we use the so-called Asimov data set [50]. We take $n_j \rightarrow b_j$ in the case of exclusion and $n_j \rightarrow s_j + b_j$ in the case of discovery. Given this, the expected exclusion significance $E[Z_e]$ is given by [50]

$$E[Z_e] = \sqrt{2 \left[\sum_{j=1}^N \left(s_j + b_j \ln \left(\frac{b_j}{b_j + s_j} \right) \right) \right]}. \quad (3.6)$$

An expected exclusion significance at the 95% CL corresponds to $E[Z_e] = 1.64$. The expected discovery significance $E[Z_0]$ is given by [50]

$$E[Z_0] = \sqrt{-2 \left[\sum_{j=1}^N \left(s_j + (b_j + s_j) \ln \left(\frac{b_j}{b_j + s_j} \right) \right) \right]}. \quad (3.7)$$

An expected discovery significance at the $n\sigma$ level corresponds to $E[Z_e] = n$.

3.3 Event Selection & Binning Scheme

The event selection and binning scheme used in our sensitivity calculations for a future collider is guided by the latest ATLAS [33, 41] and CMS [36] searches. Firstly, we scale our cut

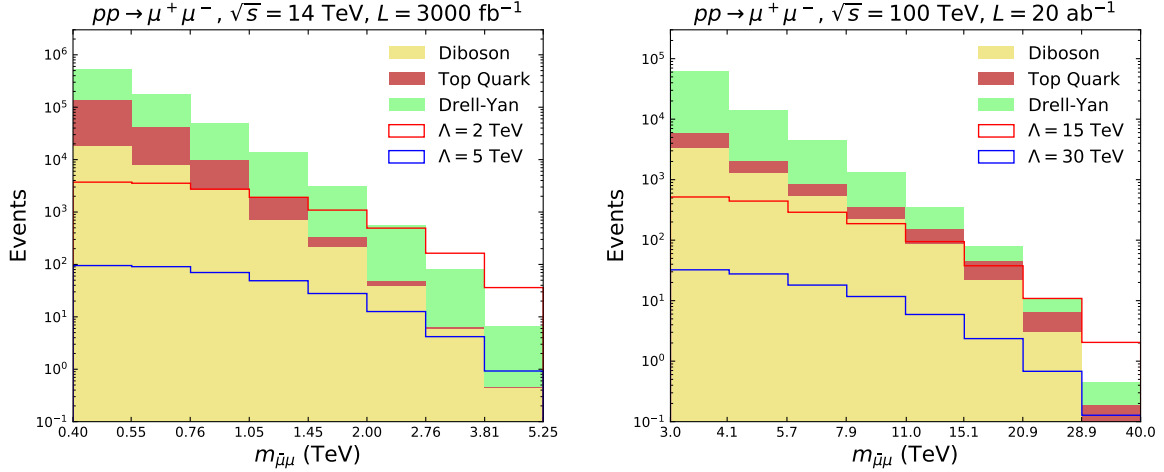


Figure 5: Dimuon invariant mass distributions including both the signal and SM background at $\sqrt{s} = 14$ TeV (left) and $\sqrt{s} = 100$ TeV (right) using the binning scheme detailed in Sec. 3.3.

on the transverse momentum p_T of the muons linearly with the c.o.m energy of the given collider considered. Thus, we take $p_T = \sqrt{s}/250$ in line with the CMS [36] selection at $\sqrt{s} = 13$ TeV. Secondly, we alter our cut on the pseudo rapidity $|\eta|$ of the muons. When considering the $\sqrt{s} = 14$ TeV HL-LHC we take $|\eta| < 2.5$ in line with ATLAS and CMS detector configurations; however, for a future collider with $\sqrt{s} > 14$ TeV we take $|\eta| < 4.0$ as is done in [26].

Both the CMS [36] and ATLAS [33] searches for contact interactions at $\sqrt{s} = 13$ TeV impose a minimum cut on the dimuon invariant mass of $m_{\mu\mu}^{\min} = 0.4$ TeV. Given this, to define our binning scheme we take $m_{\mu\mu}^{\min} = 0.43$ TeV at $\sqrt{s} = 14$ TeV and $m_{\mu\mu}^{\min} = 3$ TeV at $\sqrt{s} = 100$ TeV; here, we have loosely scaled up the minimum cut on $m_{\mu\mu}$ with \sqrt{s} with respect to $m_{\mu\mu}^{\min} = 0.4$ TeV at $\sqrt{s} = 13$ TeV. It is important to include as many signal events into our sensitivity calculations as possible. Whilst the EFT signal tends to dominate in the high invariant mass region, if $m_{\mu\mu}^{\min}$ is chosen to be too large then large numbers of signal events can be discarded and sensitivity is reduced. Hence, we find the mentioned minimum cuts on $m_{\mu\mu}$ at $\sqrt{s} = 14$ and 100 TeV give the optimal significance and including events with lower invariant masses has no significant effect, as the SM background dominates in this region.

The latest CMS (ATLAS) searches define 8 (6) bins of increasing width above 400 GeV². Given this, we consider 8 logarithmic spaced bins in the interval $[m_{\mu\mu}^{\min}, m_{\mu\mu}^{\max}]$ ³. Whilst both [33] and [36] take $m_{\mu\mu}^{\max} = 6$ TeV it is noted that, the value of $m_{\mu\mu}^{\max}$ cannot be chosen to be arbitrarily large. This point is discussed in more detail in Sec. 3.4. Fig. 5 shows invariant mass distributions at $\sqrt{s} = 14$ TeV and $\sqrt{s} = 100$ TeV using the event simulation described in Sec. 3.1 and the binning scheme and event selection described above. Here we have taken $m_{\mu\mu}^{\max}$ to be 5.25 TeV and 40 TeV respectively. This is done without regard for the validity of the EFT in order to present a large region of the invariant mass spectrum.

²The most recent inclusive ATLAS search [41] using 139 ab^{-1} of data uses a single bin above $m_{\mu\mu} > 2$ TeV. We find that using multiple bins over a larger range in $m_{\mu\mu}$ gives better sensitivity.

³Bins with constant widths have also been considered and only a minor reduction in the expected significance is seen.

3.4 Unitarity Constraints and EFT Validity

When defining our event selection, it is important to note that the value of $m_{\bar{\mu}\mu}^{\max}$ cannot be taken to be arbitrarily large. Requiring the EFT amplitude to respect tree-level unitarity implies [30]

$$m_{\bar{\mu}\mu} < \sqrt{\frac{4\pi}{\sqrt{3}}} \Lambda \equiv \Lambda_*. \quad (3.8)$$

Whenever $m_{\bar{\mu}\mu}$ becomes larger than Λ_* our description of new physics as a dimension-6 effective operator necessarily breaks down. Here, contributions from higher orders in perturbation theory, higher-dimensional operators or insertions of multiple operators, and/or the appearance of new on-shell degrees of freedom become as important as our tree-level signal.

In concrete UV completions of the EFT, the tree-level unitary bound may be reached at lower values of $m_{\bar{\mu}\mu}$. For example, in simplified Z' models [30]

$$m_{\bar{\mu}\mu} < m_{Z'} < \sqrt{\frac{2\pi}{\sqrt{3}}} \Lambda, \quad (3.9)$$

where $m_{Z'}$ is the mass of the Z' and the final bound is the tree-level unitarity constraint calculated in the Z' model. The fact that this bound is below Λ_* results from multiple channels (such as $b\bar{s} \rightarrow s\bar{b}$) being mediated by the same Z' couplings that cause the interaction in Eq. 1.3; at low energies this situation corresponds to additional SMEFT operators not relevant to $b \rightarrow s\ell^+\ell^-$ transitions.

A related question concerns the validity of the EFT expansion in Eq. 2.1 [51, 52, 53]. In our case dimension-6 is leading (due to the negligible SM contribution to $\bar{b}s \rightarrow \mu^+\mu^-$), and the relevant comparison is with dimension-8 operators. This is necessarily model-dependent. For tree-level mediators, the EFT expansion of our signal amplitude simply reproduces the expansion of the mediator propagator in p^2/M^2 , where M is the mediator mass. For an s -channel mediator (Z'), the resulting bound amounts to requiring that the dimuon invariant mass is less than the mediator mass. For a Z' , this simply means that the signal window must exclude the Z' peak in order to remain in the tail (first inequality in Eq. 3.9). The corresponding cut for a leptoquark mediator is on the value of $|t|$, which is a function of both the dimuon mass and the rapidity and therefore is less intuitive; however, as $|t| \leq s$ for $2 \rightarrow 2$ scattering, the cut $m_{\bar{\mu}\mu} < m_{\text{LQ}}$, while conservative, still ensures validity of the EFT expansion. The Z' case is worked out in Appendix B in detail in the EFT language, and the leptoquark case described qualitatively.

In the following, we give all exclusion and discovery limits as a function of $m_{\bar{\mu}\mu}^{\max}$ and we will highlight the regions in which tree-level unitarity is violated in the EFT (new physics described by a dim-6 effective operator) and under the assumption the $bs\mu\mu$ contact interaction is mediated by a Z' .

4 Results

In this section we investigate the exclusion and discovery potential of a future collider to the $bs\mu\mu$ contact interactions that define our signal Eq. 1.3. We first give updated bounds at the LHC before moving to the proposed FCC-hh and beyond. We give all 95% exclusion limits and 5σ discovery sensitivities in terms of Λ . In accordance with Sec. 3.4 we give the limits and

	95% Exclusion				5 σ Discovery			
\sqrt{s} (TeV)	13			14	13			14
L (fb $^{-1}$)	36	139	3000	3000	36	139	3000	3000
Λ (TeV) ($\epsilon = 0.75$)	2.3	2.7	4.1	4.2	1.7	2.1	3.1	3.2
Λ (TeV) ($\epsilon = 0.965$)	2.4	2.9	4.3	4.5	1.8	2.2	3.2	3.4

Table 2: 95% exclusion limits and 5 σ discovery sensitivities for Λ at the LHC. At $\sqrt{s} = 14$ TeV the event selection detailed in Sec. 3.3 is used with $m_{\mu\mu}^{\max} = 5.25$ TeV. For $\sqrt{s} = 13$ TeV, the cuts on the muon are taken directly from [41, 36] in conjunction with the binning scheme detailed in Sec. 3.3 with $m_{\mu\mu}^{\max} = 4.5$ TeV. Both values of $m_{\mu\mu}^{\max}$ have been chosen to maximise sensitivity whilst still lying comfortably below the constraint imposed by tree-level unitarity of the EFT amplitude Eq. 3.8 (as well as that of a simplified Z' model Eq. 3.9).

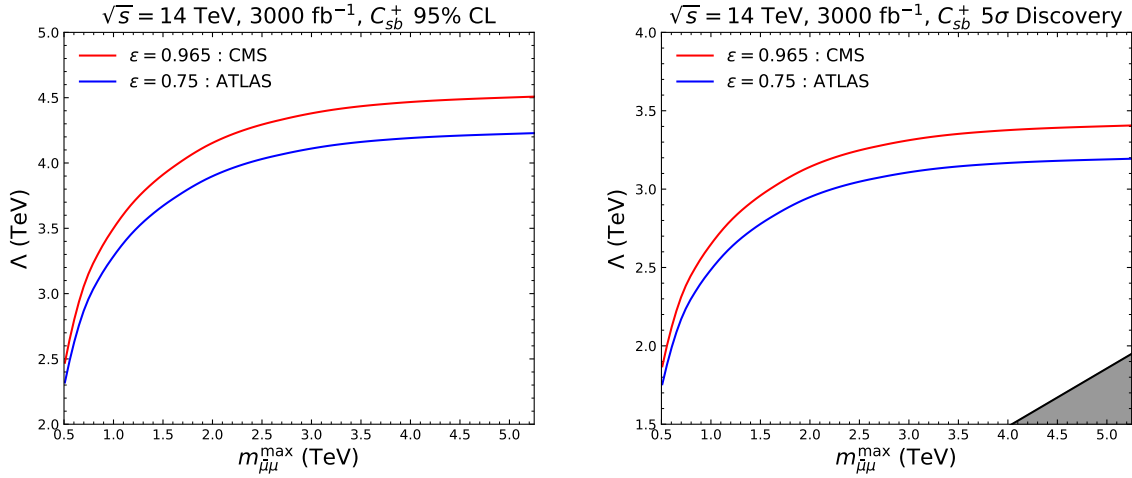


Figure 6: 95% exclusion limits and 5 σ discovery sensitivities for Λ as a function of $m_{\mu\mu}^{\max}$ at the $\sqrt{s} = 14$ TeV HL-LHC using $L = 3000$ fb $^{-1}$. The dark grey shaded region highlights the region in which tree-level unitarity of the EFT is violated (see Eq. 3.8).

sensitivities to Λ as either a function of $m_{\mu\mu}^{\max}$ or for a the value of $m_{\mu\mu}^{\max}$ that saturates the unitary constraint Eq. 3.8.

4.1 Sensitivity at the LHC

The sensitivity of the $\sqrt{s} = 13$ TeV LHC to the $bs\mu\mu$ contact interactions Eq. 1.3 using an inclusive dimuon final state has been investigated in [31]. Here 95% exclusion limits have been obtained from a collider recast based on [33] using 36 fb $^{-1}$ of data along with a projection for the HL-LHC at $\sqrt{s} = 13$ TeV. It is seen that the LHC (HL-LHC) can exclude $\Lambda = 2.5$ (4.1) TeV at the 95% CL [31]. To this end, we first rederive the results presented in [31], here including NLO effects to the EFT signal. We find a good agreement with [31] where the slight difference can be attributed to difference in our binning scheme and inclusion of detector effects. We then update the exclusion limits to include the $\sqrt{s} = 13$ TeV LHC with $L = 140$ fb $^{-1}$, the most recent LHC data set, as-well as giving projections at the 14 TeV HL-LHC. In addition to 95% exclusion limits, we also derive the value of Λ needed for 5 σ discovery. Our results are detailed in Table 2, where we consider two different muon identification and reconstruction efficiencies corresponding to the CMS or ATLAS detector.

In Table 2 it is seen that the $\sqrt{s} = 14$ TeV HL-LHC can exclude $\Lambda = 4.5$ TeV at the 95% CL and can discover $\Lambda = 3.4$ TeV at the 5σ level. A more detailed presentation of these results is shown in Fig. 6 where the exclusion limits and discovery sensitivities for Λ are given as a function of an upper cut of the dimuon invariant mass. We can see that the limits on Λ lie well below the unitarity bound Eq. 3.8 even when $m_{\mu\mu}^{\max} = 5.25$ TeV.

In both the cases of 95% exclusion and 5σ discovery, the sensitivity does not significantly change when dimuon events with $m_{\mu\mu} \gtrsim 3$ TeV are discarded. Given this, if the underlying model of NP requires $m_{\mu\mu} \gtrsim 3$ TeV in order for the EFT to remain valid, then valid limits can be obtained with minimal effect on the overall sensitivity. In a scenario such as this the EFT approach can both exclude and discover areas of parameter space for a given NP model without the need for a direct search. For example, Z' bosons with $m_{Z'} > 3$ TeV can be either excluded or discovered. Alternatively, if the underlining NP model requires a cut on the dimuon invariant mass stronger than 3 TeV then the actual sensitivity of the $\sqrt{s} = 14$ TeV HL-LHC can be significantly lower than that detailed in Table 2.

4.2 Sensitivity at the FCC-hh

Here we present 95% exclusion limits and 5σ discovery sensitivities at a future $\sqrt{s} = 100$ TeV proton-proton collider. The luminosity goal of each of the two experiments at the FCC-hh is intended to be $\sim 1 \text{ ab}^{-1}$ per year [54]. This gives a total integrated luminosity of $\sim 20 \text{ ab}^{-1}$ over the lifetime of the collider for each experiment and $\sim 40 \text{ ab}^{-1}$ if both data sets are combined. Given this, we will use $L = \{1, 20, 40\} \text{ ab}^{-1}$ as benchmark luminosities to assess the sensitivity of a $\sqrt{s} = 100$ TeV proton-proton collider to the $bs\mu\mu$ contact interaction.

In Table 3, we give the 95% exclusion limits on Λ and values of Λ needed for 5σ discovery at $\sqrt{s} = 100$ TeV. It is seen that with a maximal luminosity of $L = 40 \text{ ab}^{-1}$ the FCC-hh can exclude $\Lambda \approx 26$ TeV at the 95% CL and discover signals of $\Lambda \approx 20$ TeV at the 5σ level. A more detailed presentation of these limits is shown in Fig. 7 where we again give the limits as a function of an upper cut on the dimuon invariant mass. It is noted that the tree-level unitarity bound is more relevant at low luminosities.

Comparing Figs. 6 and 7 we see that the FCC-hh improves the sensitivity to the $bs\mu\mu$ contact interaction significantly compared to that achievable at the HL-LHC, with sensitivity improving by $\approx 500\%$. Having said this, the FCC-hh with its current design luminosity is not able to exclude or discover an EFT signal of strength of $\Lambda \approx 40$ TeV as currently suggested by the B anomalies (see Eq. 1.4). Thus, in Fig. 8, we extend beyond the design luminosity of the FCC-hh. We observe that roughly 20 times more luminosity is needed for 95% exclusion of a $\Lambda \approx 40$ TeV

	95% Exclusion			5 σ Discovery		
$L \text{ (ab}^{-1}\text{)}$	1	20	40	1	20	40
$\Lambda \text{ (TeV)}$	15.8	24.1	26.4	12.0	18.1	19.8

Table 3: 95% exclusion limits and 5σ discovery sensitivities for Λ at the $\sqrt{s} = 100$ TeV FCC-hh. The event selection used to derive these bounds is detailed in Sec. 3.3. At a luminosity of $L = 1 \text{ ab}^{-1}$ 95% exclusion limits and 5σ discovery sensitivities are obtained with $m_{\mu\mu}^{\max} = 15$ TeV. For $L = 20 \text{ ab}^{-1}$ and $L = 40 \text{ ab}^{-1}$, we take $m_{\mu\mu}^{\max} = 40$ TeV for 95% exclusion limits and $m_{\mu\mu}^{\max} = 30$ TeV for 5σ discovery. The different values of $m_{\mu\mu}^{\max}$ have been chosen to maximise sensitivity whilst still lying comfortably below the constraint imposed by tree-level unitarity of the EFT amplitude Eq. 3.8 (as well as that of a simplified Z' model Eq. 3.9).

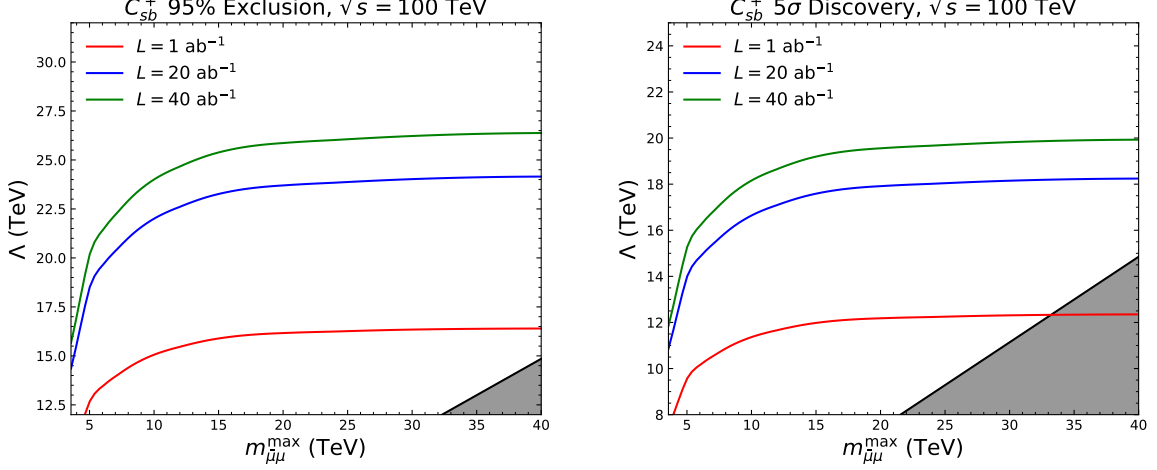


Figure 7: 95% exclusion limits and 5σ discovery sensitivities as a function of $m_{\mu\mu}^{\max}$ at $\sqrt{s} = 100$ TeV. We plot these limits for three benchmark values of the luminosities, i.e., $L = \{1, 20, 40\}$ ab^{-1} . The dark grey shaded region highlights the region in which tree-level unitarity of the EFT is violated (see Eq. 3.8).

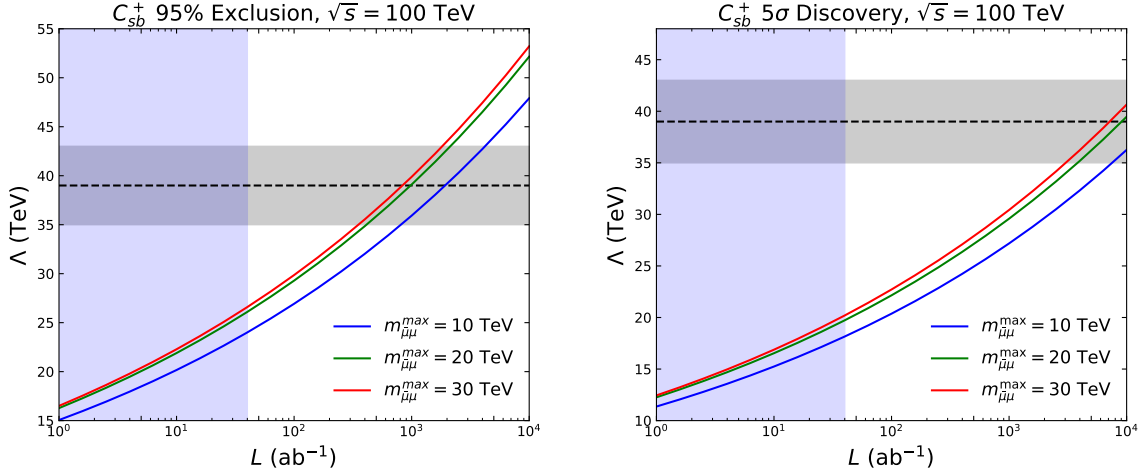


Figure 8: 95% exclusion limits and 5σ discovery sensitivities for Λ as a function of total integrated luminosity L at $\sqrt{s} = 100$ TeV. We consider three values of $m_{\mu\mu}^{\max}$. The blue shaded region signifies $L \leq 40$ ab^{-1} , the design luminosity of the FCC-hh. The dashed black line corresponds to $\Lambda = 39$ TeV with the grey shaded region corresponding to the uncertainty in Eq. 1.4.

signal and around 180 times more for 5σ discovery. However, if new measurements involving the B-anomalies point towards a lower scale of new physics then the required luminosity decreases exponentially. Signal strengths up to $\Lambda \approx 30$ TeV can be excluded or discovered with an order of magnitude less luminosity than is needed for $\Lambda \approx 40$ TeV.

4.3 Beyond the FCC-hh

In the previous two subsections, it was seen that increasing the c.o.m energy of a collider from $\sqrt{s} = 14$ TeV to $\sqrt{s} = 100$ TeV dramatically increased sensitivity. Despite this, it was seen that the FCC-hh, with its design luminosity, can neither exclude nor discover signals of order $\Lambda \approx 40$ TeV. Hence, in this section we explore the possibility of an FCC-hh with increased c.o.m energy. We first consider an FCC-hh with $\sqrt{s} > 100$ TeV and $L = 40$ ab^{-1} before varying

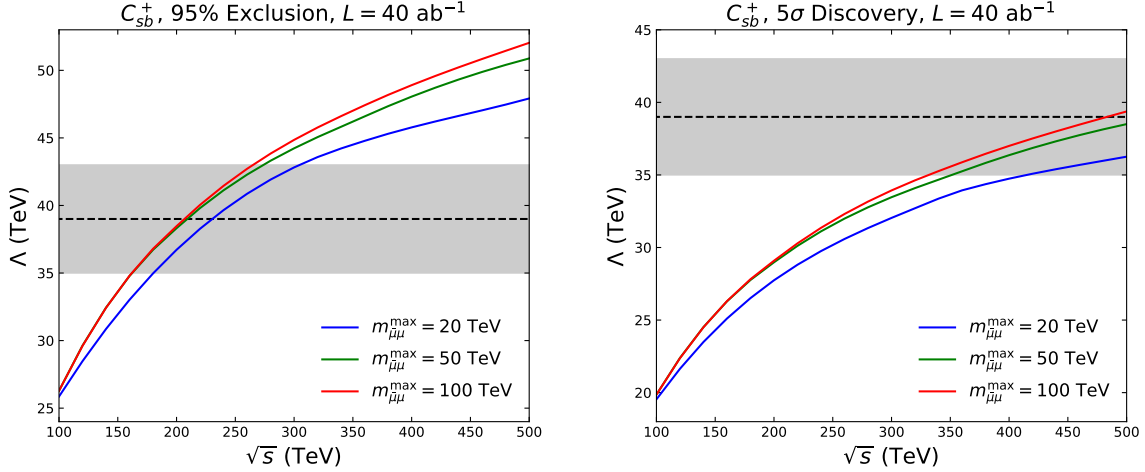


Figure 9: 95% exclusion limits and 5σ discovery sensitivities for Λ as a function of collider c.o.m energy \sqrt{s} with $L = 40 \text{ ab}^{-1}$. We consider three values of $m_{\mu\mu}^{\max}$. The dashed black line corresponds to $\Lambda = 39 \text{ TeV}$ with the grey shaded region corresponding to the uncertainty in Eq. 1.4.

both the c.o.m energy and luminosity simultaneously.

When deriving the 95% exclusion limits on and 5σ discovery sensitivities for Λ at a collider with $\sqrt{s} > 100 \text{ TeV}$ we again use the event selection detailed in Sec. 3.3. Given this, one must take care to choose a suitable value for $m_{\mu\mu}^{\min}$ at c.o.m energies higher than 100 TeV. Linearly scaling the $m_{\mu\mu}^{\min} = 0.4 \text{ TeV}$ cut used in ATLAS [33, 41] and CMS [36] with \sqrt{s} , as was done at $\sqrt{s} = 14$ and 100 TeV, generally results in a cut that is too strong and one ends up throwing away events that have a meaningful impact on the sensitivity. The reason for this is that as c.o.m energy increases the DY process and, to lesser extent, the EFT signal is suppressed by increasingly larger negative Sudakov Double Logarithms. This effectively shifts the dimuon distribution to lower values of $m_{\mu\mu}$. Hence, we find that a fixed minimum cut of $m_{\mu\mu}^{\min} = 3 \text{ TeV}$ gives the optimised sensitivity in the region of $\sqrt{s} = [100, 500] \text{ TeV}$.

Furthermore, it is seen that for a collider of $\sqrt{s} \geq 100 \text{ TeV}$ the bins that give the biggest contribution to the overall sensitivity lie approximately in the interval $m_{\mu\mu} = [7, 30] \text{ TeV}$ regardless of collider energy. Within this interval, around $\sqrt{s} = 250 \text{ TeV}$ the top and diboson backgrounds become comparable in size to the DY backgrounds and start to dominate over the DY at c.o.m energies over $\sqrt{s} = 300 \text{ TeV}$.

Fig. 9 gives the 95% exclusion limits and 5σ discovery sensitivities on Λ as a function of collider c.o.m energy with $L = 40 \text{ ab}^{-1}$. It is seen that twice the c.o.m energy is needed to exclude signals of order $\Lambda \approx 40 \text{ TeV}$ at the 95% CL. Additionally, 5 times the center of mass energy is needed for 5σ discovery. In light of this, we consider the exclusion and discovery potential of a future collider with variable luminosity and c.o.m energy. Our findings are presented in Fig. 10.

5 Conclusions

In this work we investigated the sensitivity of a future proton-proton collider to new physics indicated by the long-standing rare B -decay anomalies. We kept our analysis model-independent and conservative by only considering the minimal effective contact interaction required by the data, $1/\Lambda^2(\bar{b}_L\gamma_\mu s_L)(\bar{\mu}_L\gamma^\mu\mu_L)$. Current B -physics data indicates $\Lambda = 39 \pm 4 \text{ TeV}$, which implies that the mass of the mediators could be above 100 TeV, potentially putting them out of reach

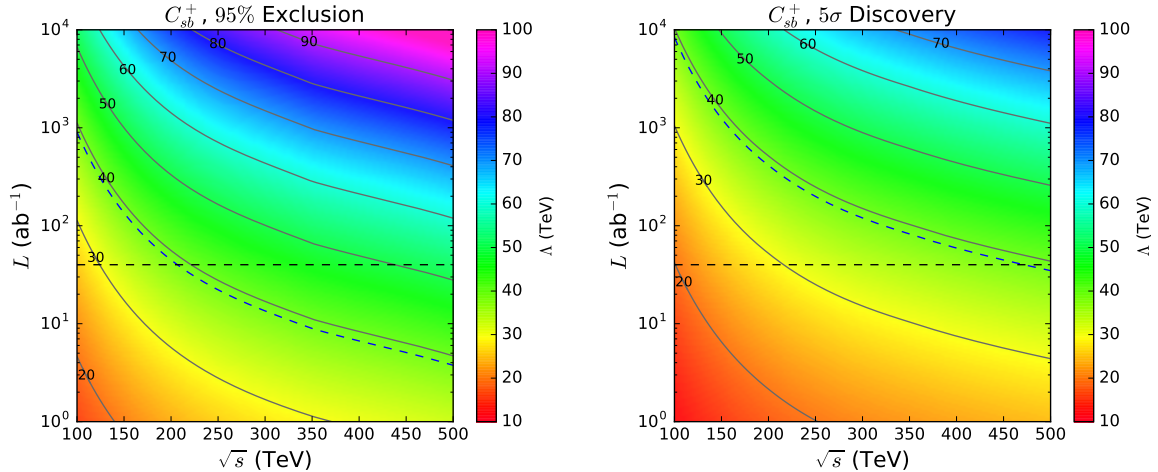


Figure 10: 95% exclusion limits and 5σ discovery sensitivities for Λ as a function of both collider c.o.m energy \sqrt{s} and luminosity $L = 40 \text{ ab}^{-1}$. Here $m_{\mu\mu}^{\text{max}}$ is set to the tree level unitarity limit in Eq. 3.8. The horizontal black dashed line gives the maximal design luminosity at the FCC-hh. The blue dashed contour corresponds to $\Lambda = 39 \text{ TeV}$, the current value of Λ suggested by the B-anomalies.

for direct searches even at the FCC-hh. Given this, we have derived both exclusion limits and discovery sensitivities for the contact interaction itself at pp colliders at various energies and luminosities, based on the tail of the inclusive dimuon invariant mass distribution. In deriving these results, we have included NLO QCD and EW corrections to the EFT signal, as well as to the dominant background component. We validated our modeling of the SM background against the current ATLAS and CMS searches and employed an optimized binning scheme. We take into account the requirements of unitarity bounds on our event selection.

We find that the $\sqrt{s} = 14 \text{ TeV}$ HL-LHC with $\mathcal{L} = 3000 \text{ fb}^{-1}$ can exclude EFT signals of strength $\Lambda = 4.5 \text{ TeV}$ at 95% CL. This compares to a limit $\Lambda = 3.9 \text{ TeV}$ obtained in [31] for $\mathcal{L} = 3000 \text{ fb}^{-1}$ and $\sqrt{s} = 13 \text{ TeV}$ and entails a cancellation between the NLO-QCD and EW corrections, as well as our inclusion of detector effects. The exclusion reach increases to $\Lambda = 26 \text{ TeV}$ when considering the $\sqrt{s} = 100 \text{ TeV}$ FCC-hh with its projected luminosity of 40 fb^{-1} . The discovery potential of the FCC-hh is also significantly stronger than that of the HL-LHC, $\Lambda = 20 \text{ TeV}$ compared to $\Lambda = 3.4 \text{ TeV}$. All limits are subject to the validity of the EFT expansion, which depends on the UV physics underlying the contact interactions. For example, in a Z' model the dimuon mass must simply be restricted to be sufficiently below the Z' mass. We quantify the reduction of Λ for various choices of upper limits on the dimuon mass.

Probing a value of $\Lambda \approx 39 \text{ TeV}$ as suggested by the B-anomalies would be possible with a machine with higher energy and/or luminosity than the FCC-hh, as we have investigated for a wide range of energies and luminosities (See Fig. 10). For example, a $\sqrt{s} = 100 \text{ TeV}$ collider would require a luminosity of $L \gtrsim 770 \text{ ab}^{-1}$, for a 95% exclusion of a $\Lambda = 39 \text{ TeV}$ signal, whereas a pp machine with $L = 40 \text{ ab}^{-1}$ would require a c.o.m energy of $\sqrt{s} \gtrsim 200 \text{ TeV}$. Discovery can be achieved with $L \gtrsim 7100 \text{ ab}^{-1}$ at $\sqrt{s} = 100 \text{ TeV}$ or $\sqrt{s} \gtrsim 470 \text{ TeV}$ at a collider with $L = 40 \text{ ab}^{-1}$. While these results may appear disillusioning at first, we remind the reader that we have been maximally conservative in our signal model: a concrete BSM model will invariably bring additional interactions, even if the mediators are too heavy for direct searches. It may moreover be possible to improve the sensitivity by considering a more complex final state with a reduced SM background. For example, for the (HL-)LHC, the authors of [34] find that an exclusive $\mu^+\mu^-b$ search can improve sensitivity to a $bs\mu\mu$ contact interaction over that

of an inclusive dimuon search. As such, we consider the question of whether a “no-lose” case can be constructed for a 100 TeV collider based on the rare B -decay anomalies an open one. A comprehensive case would combine contact interaction searches (for heavy mediators) with direct searches (for lighter mediators). We leave such studies for future work.

Acknowledgements

We thank Andrea Banfi and Jonas Lindert for many fruitful discussions throughout this project. CKK thanks Riccardo Torre for a helpful discussion regarding EFT validity. We thank Yoav Afik for clarifying several points regarding [34, 35]. SJ acknowledges support by the UK Science and Technology Facilities Council (STFC) under Consolidated Grants ST/P000819/1 and ST/T00102X/1. BG acknowledges support by a PhD studentship from the UK STFC and the School of Mathematical and Physical Sciences at the University of Sussex. SK acknowledges support by DOE grant DE-SC0011784. CKK acknowledges support from the Royal Society and SERB (under the Newton International Fellowship programme Grant No. NF171488) during the part of this project.

Note Added: After submission of this paper to the arXiv, A. Greljo informed us of an ongoing study of $bs\mu\mu$ contact interactions at future colliders.

Appendix A R_2 terms for the NLO EFT signal

Over the last decade significant advancements have been made in the automated computation of one loop amplitudes. A key observation is the fact that any one loop amplitude \mathcal{M} can be written as [55]

$$\mathcal{M} = \sum_i d_i \text{Box}_i + \sum_i c_i \text{Triangle}_i + \sum_i b_i \text{Bubble}_i + \sum_i a_i \text{Tadpole}_i + R \quad (\text{A.1})$$

where Box, Triangle, Bubble and Tadpole are known one-loop scalar integrals and R is a rational term. The OPP method [56, 55, 57] offers an effective way to compute the coefficients d_i, c_i, b_i, a_i and has been implemented in MADLOOP [58] as a part of the MADGRAPH [42, 43] framework. Despite this, the automated computation of one loop amplitudes still needs extra information that must be added to a given model by hand. The first of these missing pieces are the UV counter terms arising from the given renormalisation procedure. The second are the so called R_2 terms contained within the rational term R in Eq. A.1. Since the operators that generate the EFT signal are non-renormalisable, we are only concerned with the R_2 terms.

To evaluate loop amplitudes we use dimensional regularisation and hence work in $d = 4 + \varepsilon$ space-time dimensions. Here, all quantities ‘in the loop’ such as the loop momenta, the metric and Dirac matrices are d -dimensional whereas all external momentum vectors only have non-zero 4-dimensional components. In d -dimensions any one loop amplitude can be expressed as a sum of amplitudes of the form [55]

$$\mathcal{M}(q) = \int \frac{d^d q}{(2\pi)^d} \frac{N(q)}{D_0 D_1 \dots D_n} \quad (\text{A.2})$$

where

$$D_i = (q + \bar{p}_i)^2 - m_i^2. \quad (\text{A.3})$$

Here, q is the loop momenta, \bar{p}_i is a sum of external momenta and m_i are the masses of the particles in the loop.

Any d -dimensional space-time vector x can be split into a 4-dimensional and ε -dimensional part such that $x = \bar{x} + \tilde{x}$. Here a bar indicates the 4-dim part and a tilde the ε -dim. Given this, the numerator in Eq. A.2 can be split such that [55]

$$N(q) = \bar{N}(\bar{q}) + \tilde{N}(\tilde{q}^2, \bar{q}, \varepsilon). \quad (\text{A.4})$$

The R_2 terms are the finite parts of the loop amplitude stemming from the ε -dimensional part of the numerator and are defined for each loop integral of the form in Eq. A.2 such that [55]

$$R_2 = \lim_{\varepsilon \rightarrow 0} \int \frac{d^d q}{(2\pi)^d} \frac{\tilde{N}(\tilde{q}^2, \bar{q}, \varepsilon)}{D_0 D_1 \dots D_n}. \quad (\text{A.5})$$

When working within dimensional regularisation, a scheme for dealing with the d -dimensional Dirac matrices must be chosen. Given this, we work in the naive dimensional regularisation (NDR) scheme. This is done to be consistent with the default SM UFO model used by MadGraph to which we add the relevant EFT operators. In the NDR scheme, γ^5 is defined to anticommute with all of the Dirac matrices such that

$$\{\bar{\gamma}_\mu, \gamma^5\} = 0 \quad \{\tilde{\gamma}_\mu, \gamma^5\} = 0. \quad (\text{A.6})$$

Whilst computations are generally simpler in the NDR scheme compared to others, this scheme does contain algebraic inconsistencies which, at first glance, seem to be troublesome when considering the EFT signal. In particular, one of the main shortcomings of the NDR scheme is the fact that the expression $\text{tr}(\gamma_\mu \gamma_\nu \gamma_\rho \gamma_\sigma \gamma^5)$ is ambiguous. Traces of this form occur whenever a Feynman diagram contains a closed fermion loop. Whilst it is the case that the NLO EW corrections to the EFT signal do indeed involve closed fermion loops, see Tab. 4 and 5, it is also the case that two of the space-time indices on the Dirac matrices within the trace are always contracted during the calculation. This contraction of indices leads to unambiguous results in all instances and allows consistent use the NDR scheme.

To fix our conventions and notations we give the Feynman rules used in our NLO calculations:

$$\begin{aligned} \mu \xrightarrow[p]{V, W} \nu &= \frac{-i\eta_{\mu\nu}}{p^2 - m_{V,W}^2}, & \xrightarrow[p]{d_n^i, u_n^i, \mu_n^-, \nu_\mu} &= \frac{i\not{p}^2}{p^2}, \\ V \xrightarrow{\quad} \begin{array}{c} d_L^i \\ \swarrow \\ \searrow \\ d_L^i \end{array} &= i\gamma_\mu(v_d + a_d\gamma^5), & V \xrightarrow{\quad} \begin{array}{c} u_L^i \\ \swarrow \\ \searrow \\ u_L^i \end{array} &= i\gamma_\mu(v_u + a_u\gamma^5), \\ W \xrightarrow{\quad} \begin{array}{c} d_L^j \\ \swarrow \\ \searrow \\ u_L^i \end{array} &= \frac{ie}{2\sqrt{2}\sin\theta_W}\gamma_\mu(1 - \gamma^5)V_{ij}, \end{aligned} \quad (\text{A.7})$$

$$\begin{aligned}
V \text{ (wavy)} \begin{array}{l} \nearrow \mu_n^- \\ \searrow \mu_n^- \end{array} &= i\gamma_\mu(v_{\mu,n} + a_{\mu,n}\gamma^5), & V \text{ (wavy)} \begin{array}{l} \nearrow \nu_\mu \\ \searrow \nu_\mu \end{array} &= i\gamma_\mu(v_\nu + a_\nu\gamma^5), \\
W \text{ (wavy)} \begin{array}{l} \nearrow \mu^- \\ \searrow \nu_\mu \end{array} &= \frac{ie}{2\sqrt{2}\sin\theta_W}\gamma_\mu(1 - \gamma^5).
\end{aligned}$$

Above, V is a neutral SM gauge boson, i.e., $V = \{\gamma, g, Z\}$, W is one of the charged SM W^\pm bosons and $m_{V,W}$ is the mass of the V or W . In regards to indices, $n = \{L, R\}$, indicating the chirality of a given fermion, and i and j run over the generations of quarks. It is noted that all quarks are taken to be massless except for the top quark which we do not consider here.

The LO Feynman diagram for the $\bar{d}_L^j d_L^i \rightarrow \mu_L^+ \mu_L^-$ transition is given by


(A.8)

The corresponding LO amplitude \mathcal{M}_{LO} can be explicitly written as

$$i\mathcal{M}_{\text{LO}} = iC_{ij}^+ \bar{d}_L^j(p_2) \gamma^\nu d_L^i(p_1) \bar{\mu}_L(p_4) \gamma_\nu \mu_L(p_3). \quad (\text{A.9})$$

The one loop corrections to the EFT signal can be categorized into four types⁴. The four types of diagrams and the resulting R_2 terms are detailed in Tab. 4. It is noted however, that there are actually four equivalent diagrams of type C for both $V = \gamma$ and $V = Z$ for a given choice of i and j . These four diagrams correspond to the four possible configurations in which V exchange can take place between one of the initial state quarks and one of the final state muons. Even though only one of the four diagrams is shown here, the R_2 terms arising from each of these four diagrams are equivalent.

Finally, it is noted that there are one loop EW diagrams proportional to C_{sb}^+ that do not contribute to $\bar{d}_L^j d_L^i \rightarrow \mu_L^+ \mu_L^-$ but still contribute to $pp \rightarrow \mu^+ \mu^-$. For completeness, we give the R_2 terms arising from these diagrams. The first of these diagrams arises from diagrams of type D in Tab. 4 in which the final state muons are right-handed. This diagram is proportional to

$$i\mathcal{M}_{\text{LR}} = iC_{ij}^+ \bar{d}_L^j(p_2) \gamma^\nu d_L^i(p_1) \bar{\mu}_R(p_4) \gamma_\nu \mu_R(p_3). \quad (\text{A.10})$$

We label this a diagram of type E and its R_2 term is given in Tab. 5.

The remaining diagrams involve initial state up-type quarks and are proportional to either

$$i\mathcal{M}^{\text{up}} = iC_{ij}^+ \bar{u}_L^l(p_2) \gamma^\nu u_L^k(p_1) \bar{\mu}_L(p_4) \gamma_\nu \mu_L(p_3) \quad (\text{A.11})$$

⁴It is noted that if $i = j$ then there are additional diagrams that are not presented here.

or

$$i\mathcal{M}_{\text{LR}}^{\text{up}} = iC_{ij}^+ \bar{u}_L^l(p_2) \gamma^\nu u_L^k(p_1) \bar{\mu}_R(p_4) \gamma_\nu \mu_R(p_3). \quad (\text{A.12})$$

The first of these diagrams, type F, arise from the flavour changing interaction of the W . The remaining diagrams involve the presence of neutrinos in loops and originate from the operator structure seen in Eq. 2.5. Again, the R_2 terms for all diagrams are given in Tab. 5.

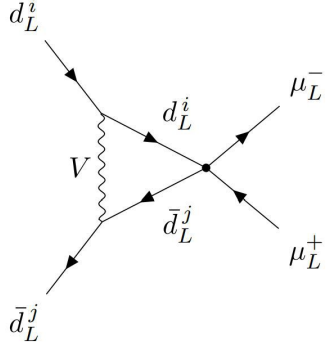
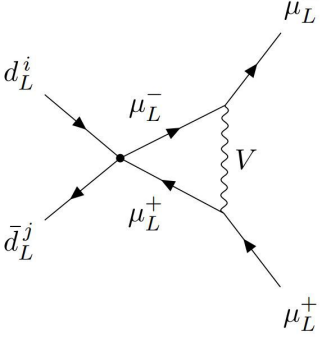
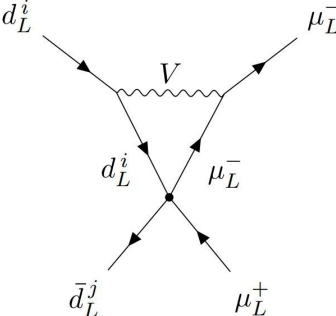
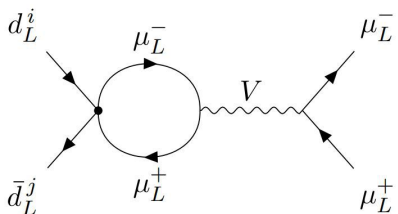
Type	Diagram	R_2
A		$\frac{i}{8\pi^2} (v_d - a_d)^2 \mathcal{M}_{\text{LO}}$
B		$\frac{i}{8\pi^2} (v_{\mu,L} - a_{\mu,L})^2 \mathcal{M}_{\text{LO}}$
C		$\frac{i}{8\pi^2} (v_{\mu,L} - a_{\mu,L})(v_d - a_d) \mathcal{M}_{\text{LO}}$
D		$\frac{-i}{48\pi^2} \frac{m_{\bar{\mu}\mu}^2}{(m_{\bar{\mu}\mu}^2 - m_V^2)} (v_{\mu,L} - a_{\mu,L})^2 \mathcal{M}_{\text{LO}}$

Table 4: The one loop corrections to the EFT signal that give a contribution to the $\bar{d}_L^j d_L^i \rightarrow \mu_L^+ \mu_L^-$ scattering amplitude. The R_2 terms corresponding to these diagrams are given in the final column. There are four equivalent diagrams of type C but only one is shown here.

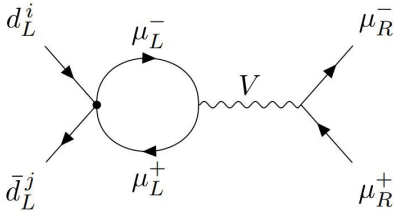
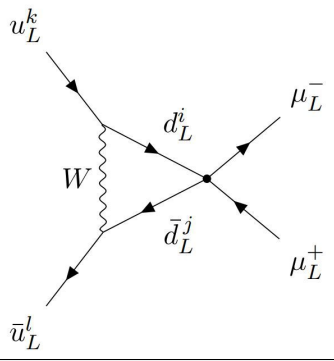
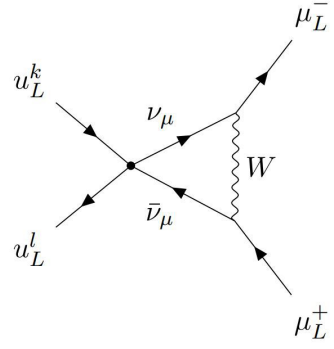
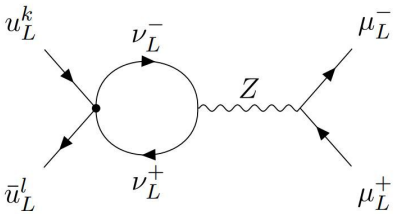
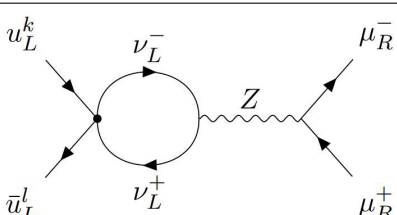
Type	Diagram	R_2
E		$\frac{-i}{48\pi^2} \frac{m_{\bar{\mu}\mu}^2}{(m_{\bar{\mu}\mu}^2 - m_V^2)} v_{\mu,R}(v_{\mu,L} - a_{\mu,L}) \mathcal{M}_{\text{LR}}$
F		$\frac{-ie^2}{8\pi^2 \sin^2 \theta_W} V_{ki}^* V_{lj} \mathcal{M}^{\text{up}}$
G		$\frac{-ie^2}{8\pi^2 \sin^2 \theta_W} V_{ki}^* V_{lj} \mathcal{M}^{\text{up}}$
H		$\frac{-i}{48\pi^2} \frac{m_{\bar{\mu}\mu}^2}{(m_{\bar{\mu}\mu}^2 - m_Z^2)} (v_\nu - a_\nu)(v_{\mu,L} - a_{\mu,L}) V_{ki}^* V_{lj} \mathcal{M}^{\text{up}}$
I		$\frac{-i}{48\pi^2} \frac{m_{\bar{\mu}\mu}^2}{(m_{\bar{\mu}\mu}^2 - m_Z^2)} v_{\mu,R}(v_\nu - a_\nu) V_{ki}^* V_{lj} \mathcal{M}_{\text{LR}}^{\text{up}}$

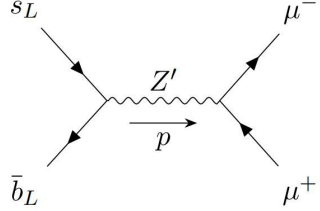
Table 5: The one loop corrections to the EFT signal that give a contribution to the $pp \rightarrow \mu^+ \mu$ scattering amplitude but are not proportional to \mathcal{M}_{LO} . The R_2 terms corresponding to these diagrams are given in the final column.

Appendix B EFT Validity: Simplified Z' Model

In this section we work out the EFT expansion and partial-wave unitarity bound for a Z' mediator (cf Sec. 3.4). The minimum terms needed for a Z' to mediate an interaction between left-handed b and s quarks and muons are

$$\mathcal{L}_{\text{int}} = g_{\mu\mu} Z'_\nu \bar{\mu}_L \gamma^\nu \mu_L - g_{sb} Z'_\nu \bar{b}_L \gamma^\nu s_L - g_{sb}^* Z'_\nu \bar{s}_L \gamma^\nu b_L. \quad (\text{B.1})$$

For simplicity, we take the couplings $g_{\mu\mu}$ and g_{sb} to be real such that $g_{\mu\mu} > 0$ and $g_{sb} < 0$. Given Eq. B.1, the LO amplitude for the process $b_L s_L \mu_L^+ \mu_L^-$ is given by



$$= \frac{-ig}{p^2 - m_{Z'}^2} \bar{b}_L(p_1) \gamma^\nu s_L(p_2) \bar{\mu}_L(p_3) \gamma_\nu \mu_L(p_4) \quad (\text{B.2})$$

where $g = g_{sb} g_{\mu\mu}$.

Expanding the factor multiplying the spinor structure in Eq. B.2 in powers of p^2 , we have

$$\frac{-ig}{p^2 - m_{Z'}^2} = \frac{ig}{m_{Z'}^2} + \frac{igp^2}{m_{Z'}^4} + \frac{igp^4}{m_{Z'}^6} + \frac{igp^6}{m_{Z'}^8} + \dots \quad (\text{B.3})$$

We see that the higher-order terms can be neglected provided $p^2 \ll m_{Z'}^2$, which considering $p^2 = m_{\bar{\mu}\mu}^2$ is equivalent to $m_{\bar{\mu}\mu} \ll m_{Z'}$. Hence, in the region where $m_{Z'} \gg m_{\bar{\mu}\mu}$, the signal amplitude is accurately described by the leading term, which is reproduced by the dim-6 effective operator in Eq. 2.7, with

$$\frac{g}{m_{Z'}^2} = C_{sb}^+ = \frac{1}{\Lambda^2}. \quad (\text{B.4})$$

Expressed in terms of Λ , the EFT is applicable provided $m_{\bar{\mu}\mu} \ll \sqrt{g}\Lambda$. Together with the partial wave unitarity bound Eq. 3.9, we see that g cannot be greater than $2\pi/\sqrt{3}$.

We can reproduce the higher-order terms in the expansion (Eq. B.3) in the EFT by matching them to effective operators of dimension greater than 6. Using notation analogous to that in Sec. 2, the relevant operators at dimension-8 are [59, 60, 61]

$$\begin{aligned} \mathcal{L}^{\text{SMEFT}} \supset & \frac{c_{Q_{ij}L_{kl}}^{(3,1)}}{\hat{\Lambda}^4} (\partial_\nu (\bar{Q}_i \gamma_\mu \sigma^a Q_j)) (\partial^\nu (\bar{L}_k \gamma^\mu \sigma_a L_l)) + \frac{c_{Q_{ij}L_{kl}}^{(1,1)}}{\hat{\Lambda}^4} (\partial_\nu (\bar{Q}_i \gamma_\mu Q_j)) (\partial^\nu (\bar{L}_k \gamma^\mu L_l)) \\ & + \frac{c_{Q_{ij}L_{kl}}^{(3,2)}}{\hat{\Lambda}^4} (\bar{Q}_i \gamma_\mu \overleftrightarrow{\partial}_\nu^a Q_j) (\bar{L}_k \gamma^\mu \overleftrightarrow{\partial}^{a,\nu} L_l) + \frac{c_{Q_{ij}L_{kl}}^{(1,2)}}{\hat{\Lambda}^4} (\bar{Q}_i \gamma_\mu \overleftrightarrow{\partial}_\nu Q_j) (\bar{L}_k \gamma^\mu \overleftrightarrow{\partial}^\nu L_l), \end{aligned} \quad (\text{B.5})$$

and we can change to an operator basis analogous to the (C_{ij}^+, C_{ij}^-) basis (cf Sec. 2),

$$\begin{aligned} \mathcal{L}^{\text{SMEFT}} \supset & \frac{f_{ij}^1}{\hat{\Lambda}^4} \left[\left(\bar{d}_L^i(x_1) \gamma_\mu (\partial_\nu d_L^j(x_2)) \right) + (\partial_\nu \bar{d}_L^i(x_1)) \gamma_\mu d_L^j(x_2) \right) + \\ & (\bar{\mu}_L(x_4) \gamma^\mu (\partial_\nu \mu_L(x_3)) + (\partial_\nu \bar{\mu}_L(x_4)) \gamma^\mu \mu_L(x_3)) \Big] \\ & + \frac{f_{ij}^2}{\hat{\Lambda}^4} \left[\left(\bar{d}_L^i(x_1) \gamma_\mu (\partial_\nu d_L^j(x_2)) \right) - (\partial_\nu \bar{d}_L^i(x_1)) \gamma_\mu d_L^j(x_2) \right) + \\ & (\bar{\mu}_L(x_4) \gamma^\mu (\partial_\nu \mu_L(x_3)) - (\partial_\nu \bar{\mu}_L(x_4)) \gamma^\mu \mu_L(x_3)) \Big], \end{aligned} \quad (\text{B.6})$$

where

$$f_{ij}^k = c_{Q_{ij}L_{\mu\mu}}^{(1,k)} + c_{Q_{ij}L_{\mu\mu}}^{(3,k)}. \quad (\text{B.7})$$

The $2 \rightarrow 2$ scattering amplitude \mathcal{M} calculated in the EFT through dimension-8 becomes

$$i\mathcal{M} = iA_{ij}\bar{d}_L^i(p_1)\gamma_\nu d_L^j(p_2)\bar{\mu}_L(p_3)\gamma^\nu\mu_L(p_4), \quad (\text{B.8})$$

where

$$A_{ij} = \frac{g_{ij}^+}{\hat{\Lambda}^2} + \frac{f_{ij}^1 s}{\hat{\Lambda}^4} + \frac{f_{ij}^2(-s-2t)}{\hat{\Lambda}^4}. \quad (\text{B.9})$$

Setting $\hat{\Lambda} = \Lambda$ and comparing to Eqs. B.2 and B.3, we obtain $g_{sb}^+ = f_{sb}^1 = g$ and $f_{sb}^2 = 0$, for which

$$i\mathcal{M} = \left(\frac{ig}{m_{Z'}^2} + \frac{igm_{\bar{\mu}\mu}^2}{m_{Z'}^4} \right) \bar{b}_L(p_1)\gamma_\nu s_L(p_2)\bar{\mu}_L(p_3)\gamma^\nu\mu_L(p_4) \quad (\text{B.10})$$

reproduces Eq. B.2 through the second term in the expansion Eq. B.3. To conclude this section, let us note that Eq. B.9 can capture the case of a leptoquark mediator, too, in which case $f_{sb}^1 = f_{sb}^2$, such that the dimension-8 term is proportional to t , reflecting the fact that the mediator is in the t -channel. (In this case, the EFT is valid provided $|t| < m_{LQ}^2$, which is not a simple cut on the dimuon mass.) This gives a concrete demonstration of the universal applicability of the EFT, which further extends to loop-level mediators.

References

- [1] A. Cerri et al. Report from Working Group 4: Opportunities in Flavour Physics at the HL-LHC and HE-LHC. *CERN Yellow Rep. Monogr.*, 7:867–1158, 2019. [arXiv:1812.07638](#), [doi:10.23731/CYRM-2019-007.867](#).
- [2] David London and Joaquim Matias. *B* Flavour Anomalies: 2021 Theoretical Status Report. 10 2021. [arXiv:2110.13270](#), [doi:10.1146/annurev-nucl-102020-090209](#).
- [3] Gudrun Hiller and Frank Kruger. More model independent analysis of $b \rightarrow s$ processes. *Phys. Rev.*, D69:074020, 2004. [arXiv:hep-ph/0310219](#), [doi:10.1103/PhysRevD.69.074020](#).
- [4] Li-Sheng Geng, Benjamín Grinstein, Sebastian Jäger, Shuang-Yi Li, Jorge Martin Camalich, and Rui-Xiang Shi. Implications of new evidence for lepton-universality violation in $b \rightarrow s\ell + \ell^-$ decays. *Phys. Rev. D*, 104(3):035029, 2021. [arXiv:2103.12738](#), [doi:10.1103/PhysRevD.104.035029](#).
- [5] Morad Aaboud et al. Study of the rare decays of B_s^0 and B^0 mesons into muon pairs using data collected during 2015 and 2016 with the ATLAS detector. *JHEP*, 04:098, 2019. [arXiv:1812.03017](#), [doi:10.1007/JHEP04\(2019\)098](#).
- [6] Albert M Sirunyan et al. Measurement of properties of $B_s^0 \rightarrow \mu^+\mu^-$ decays and search for $B^0 \rightarrow \mu^+\mu^-$ with the CMS experiment. *JHEP*, 04:188, 2020. [arXiv:1910.12127](#), [doi:10.1007/JHEP04\(2020\)188](#).
- [7] Roel Aaij et al. Measurement of the $B_s^0 \rightarrow \mu^+\mu^-$ decay properties and search for the $B^0 \rightarrow \mu^+\mu^-$ and $B_s^0 \rightarrow \mu^+\mu^-\gamma$ decays. *Phys. Rev. D*, 105(1):012010, 2022. [arXiv:2108.09283](#), [doi:10.1103/PhysRevD.105.012010](#).

- [8] Roel Aaij et al. Test of lepton universality in beauty-quark decays. 3 2021. [arXiv:2103.11769](#).
- [9] S. Choudhury et al. Test of lepton flavor universality and search for lepton flavor violation in $B \rightarrow K\ell\ell$ decays. *JHEP*, 03:105, 2021. [arXiv:1908.01848](#), [doi:10.1007/JHEP03\(2021\)105](#).
- [10] R. Aaij et al. Test of lepton universality with $B^0 \rightarrow K^{*0}\ell^+\ell^-$ decays. *JHEP*, 08:055, 2017. [arXiv:1705.05802](#), [doi:10.1007/JHEP08\(2017\)055](#).
- [11] A. Abdesselam et al. Test of Lepton-Flavor Universality in $B \rightarrow K^*\ell^+\ell^-$ Decays at Belle. *Phys. Rev. Lett.*, 126(16):161801, 2021. [arXiv:1904.02440](#), [doi:10.1103/PhysRevLett.126.161801](#).
- [12] Li-Sheng Geng, Benjamín Grinstein, Sebastian Jäger, Jorge Martin Camalich, Xiu-Lei Ren, and Rui-Xiang Shi. Towards the discovery of new physics with lepton-universality ratios of $b \rightarrow s\ell\ell$ decays. *Phys. Rev. D*, 96(9):093006, 2017. [arXiv:1704.05446](#), [doi:10.1103/PhysRevD.96.093006](#).
- [13] Martin Beneke, Christoph Bobeth, and Robert Szafron. Power-enhanced leading-logarithmic QED corrections to $B_q \rightarrow \mu^+\mu^-$. *JHEP*, 10:232, 2019. [arXiv:1908.07011](#), [doi:10.1007/JHEP10\(2019\)232](#).
- [14] Marzia Bordone, Gino Isidori, and Andrea Pattori. On the Standard Model predictions for R_K and R_{K^*} . *Eur. Phys. J. C*, 76(8):440, 2016. [arXiv:1605.07633](#), [doi:10.1140/epjc/s10052-016-4274-7](#).
- [15] Gino Isidori, Saad Nabeebaccus, and Roman Zwicky. QED corrections in $\bar{B} \rightarrow \bar{K}\ell^+\ell^-$ at the double-differential level. *JHEP*, 12:104, 2020. [arXiv:2009.00929](#), [doi:10.1007/JHEP12\(2020\)104](#).
- [16] Wolfgang Altmannshofer and Peter Stangl. New physics in rare B decays after Moriond 2021. *Eur. Phys. J. C*, 81(10):952, 2021. [arXiv:2103.13370](#), [doi:10.1140/epjc/s10052-021-09725-1](#).
- [17] Marcel Algueró, Bernat Capdevila, Sébastien Descotes-Genon, Joaquim Matias, and Martín Novoa-Brunet. $b \rightarrow s\ell^+\ell^-$ global fits after R_{K_S} and $R_{K^{*+}}$. *Eur. Phys. J. C*, 82(4):326, 2022. [arXiv:2104.08921](#), [doi:10.1140/epjc/s10052-022-10231-1](#).
- [18] T. Hurth, F. Mahmoudi, D. Martinez Santos, and S. Neshatpour. More Indications for Lepton Nonuniversality in $b \rightarrow s\ell^+\ell^-$. 4 2021. [arXiv:2104.10058](#), [doi:10.1016/j.physletb.2021.136838](#).
- [19] Georges Aad et al. Search for high-mass dilepton resonances using 139 fb⁻¹ of pp collision data collected at $\sqrt{s}=13$ TeV with the ATLAS detector. *Phys. Lett. B*, 796:68–87, 2019. [arXiv:1903.06248](#), [doi:10.1016/j.physletb.2019.07.016](#).
- [20] Albert M Sirunyan et al. Combination of CMS searches for heavy resonances decaying to pairs of bosons or leptons. *Phys. Lett. B*, 798:134952, 2019. [arXiv:1906.00057](#), [doi:10.1016/j.physletb.2019.134952](#).
- [21] B.C. Allanach, Ben Gripaios, and Tevong You. The case for future hadron colliders from $B \rightarrow K^{(*)}\mu^+\mu^-$ decays. *JHEP*, 03:021, 2018. [arXiv:1710.06363](#), [doi:10.1007/JHEP03\(2018\)021](#).

- [22] B.C. Allanach, Tyler Corbett, Matthew J. Dolan, and Tevong You. Hadron collider sensitivity to fat flavourful Z 's for $R_{K^{(*)}}$. *JHEP*, 03:137, 2019. [arXiv:1810.02166](#), [doi:10.1007/JHEP03\(2019\)137](#).
- [23] B.C. Allanach, J.M. Butterworth, and Tyler Corbett. Collider constraints on Z' models for neutral current B-anomalies. *JHEP*, 08:106, 2019. [arXiv:1904.10954](#), [doi:10.1007/JHEP08\(2019\)106](#).
- [24] B. C. Allanach, J. M. Butterworth, and Tyler Corbett. Large hadron collider constraints on some simple Z' models for $b \rightarrow s\mu^+\mu^-$ anomalies. *Eur. Phys. J. C*, 81(12):1126, 2021. [arXiv:2110.13518](#), [doi:10.1140/epjc/s10052-021-09919-7](#).
- [25] Shaouly Bar-Shalom, Jonathan Cohen, Amarjit Soni, and Jose Wudka. Phenomenology of TeV-scale scalar Leptoquarks in the EFT. *Phys. Rev. D*, 100(5):055020, 2019. [arXiv:1812.03178](#), [doi:10.1103/PhysRevD.100.055020](#).
- [26] B. C. Allanach, Tyler Corbett, and Maeve Madigan. Sensitivity of Future Hadron Colliders to Leptoquark Pair Production in the Di-Muon Di-Jets Channel. *Eur. Phys. J. C*, 80(2):170, 2020. [arXiv:1911.04455](#), [doi:10.1140/epjc/s10052-020-7722-3](#).
- [27] Gudrun Hiller, Dennis Loose, and Ivan Nišandžić. Flavorful leptoquarks at the LHC and beyond: spin 1. *JHEP*, 06:080, 2021. [arXiv:2103.12724](#), [doi:10.1007/JHEP06\(2021\)080](#).
- [28] Wolfgang Altmannshofer, P. S. Bhupal Dev, Amarjit Soni, and Yicong Sui. Addressing $R_{D^{(*)}}$, $R_{K^{(*)}}$, muon $g - 2$ and ANITA anomalies in a minimal R -parity violating supersymmetric framework. *Phys. Rev. D*, 102(1):015031, 2020. [arXiv:2002.12910](#), [doi:10.1103/PhysRevD.102.015031](#).
- [29] P. S. Bhupal Dev, Amarjit Soni, and Fang Xu. Hints of Natural Supersymmetry in Flavor Anomalies? 6 2021. [arXiv:2106.15647](#).
- [30] Luca Di Luzio and Marco Nardecchia. What is the scale of new physics behind the B -flavour anomalies? *Eur. Phys. J. C*, 77(8):536, 2017. [arXiv:1706.01868](#), [doi:10.1140/epjc/s10052-017-5118-9](#).
- [31] Admir Greljo and David Marzocca. High- p_T dilepton tails and flavor physics. *Eur. Phys. J.*, C77(8):548, 2017. [arXiv:1704.09015](#), [doi:10.1140/epjc/s10052-017-5119-8](#).
- [32] Simone Alioli, Marco Farina, Duccio Pappadopulo, and Joshua T. Ruderman. Catching a New Force by the Tail. *Phys. Rev. Lett.*, 120(10):101801, 2018. [arXiv:1712.02347](#), [doi:10.1103/PhysRevLett.120.101801](#).
- [33] Morad Aaboud et al. Search for new high-mass phenomena in the dilepton final state using 36 fb^{-1} of proton-proton collision data at $\sqrt{s} = 13\text{ TeV}$ with the ATLAS detector. *JHEP*, 10:182, 2017. [arXiv:1707.02424](#), [doi:10.1007/JHEP10\(2017\)182](#).
- [34] Yoav Afik, Jonathan Cohen, Eitan Gozani, Enrique Kajomovitz, and Yoram Rozen. Establishing a Search for $b \rightarrow s\ell^+\ell^-$ Anomalies at the LHC. *JHEP*, 08:056, 2018. [arXiv:1805.11402](#), [doi:10.1007/JHEP08\(2018\)056](#).
- [35] Yoav Afik, Shaouly Bar-Shalom, Jonathan Cohen, and Yoram Rozen. Searching for New Physics with $b\bar{b}\ell^+\ell^-$ contact interactions. *Phys. Lett. B*, 807:135541, 2020. [arXiv:1912.00425](#), [doi:10.1016/j.physletb.2020.135541](#).

- [36] Albert M Sirunyan et al. Search for resonant and nonresonant new phenomena in high-mass dilepton final states at $\sqrt{s} = 13$ TeV. *JHEP*, 07:208, 2021. [arXiv:2103.02708](#), [doi:10.1007/JHEP07\(2021\)208](#).
- [37] Georges Aad et al. Search for New Phenomena in Final States with Two Leptons and One or No b -Tagged Jets at $\sqrt{s} = 13$ TeV Using the ATLAS Detector. *Phys. Rev. Lett.*, 127(14):141801, 2021. [arXiv:2105.13847](#), [doi:10.1103/PhysRevLett.127.141801](#).
- [38] Guo-yuan Huang, Sudip Jana, Farinaldo S. Queiroz, and Werner Rodejohann. Probing the $RK^{(*)}$ anomaly at a muon collider. *Phys. Rev. D*, 105(1):015013, 2022. [arXiv:2103.01617](#), [doi:10.1103/PhysRevD.105.015013](#).
- [39] W. Buchmuller and D. Wyler. Effective Lagrangian Analysis of New Interactions and Flavor Conservation. *Nucl. Phys. B*, 268:621–653, 1986. [doi:10.1016/0550-3213\(86\)90262-2](#).
- [40] B. Grzadkowski, M. Iskrzynski, M. Misiak, and J. Rosiek. Dimension-Six Terms in the Standard Model Lagrangian. *JHEP*, 10:085, 2010. [arXiv:1008.4884](#), [doi:10.1007/JHEP10\(2010\)085](#).
- [41] Georges Aad et al. Search for new non-resonant phenomena in high-mass dilepton final states with the ATLAS detector. *JHEP*, 11:005, 2020. [arXiv:2006.12946](#), [doi:10.1007/JHEP11\(2020\)005](#).
- [42] J. Alwall, R. Frederix, S. Frixione, V. Hirschi, F. Maltoni, O. Mattelaer, H. S. Shao, T. Stelzer, P. Torrielli, and M. Zaro. The automated computation of tree-level and next-to-leading order differential cross sections, and their matching to parton shower simulations. *JHEP*, 07:079, 2014. [arXiv:1405.0301](#), [doi:10.1007/JHEP07\(2014\)079](#).
- [43] R. Frederix, S. Frixione, V. Hirschi, D. Pagani, H. S. Shao, and M. Zaro. The automation of next-to-leading order electroweak calculations. *JHEP*, 07:185, 2018. [arXiv:1804.10017](#), [doi:10.1007/JHEP07\(2018\)185](#).
- [44] Richard D. Ball et al. Parton distributions from high-precision collider data. *Eur. Phys. J. C*, 77(10):663, 2017. [arXiv:1706.00428](#), [doi:10.1140/epjc/s10052-017-5199-5](#).
- [45] Andy Buckley, James Ferrando, Stephen Lloyd, Karl Nordström, Ben Page, Martin Rüfenacht, Marek Schönherr, and Graeme Watt. LHAPDF6: parton density access in the LHC precision era. *Eur. Phys. J. C*, 75:132, 2015. [arXiv:1412.7420](#), [doi:10.1140/epjc/s10052-015-3318-8](#).
- [46] Georges Aad et al. Muon reconstruction and identification efficiency in ATLAS using the full Run 2 pp collision data set at $\sqrt{s} = 13$ TeV. *Eur. Phys. J. C*, 81:578, 2021. [arXiv:2012.00578](#), [doi:10.1140/epjc/s10052-021-09233-2](#).
- [47] Clement Helsens, David Jamin, Michelangelo L. Mangano, Thomas G. Rizzo, and Michele Selvaggi. Heavy resonances at energy-frontier hadron colliders. *Eur. Phys. J. C*, 79:569, 2019. [arXiv:1902.11217](#), [doi:10.1140/epjc/s10052-019-7062-3](#).
- [48] Celine Degrande, Claude Duhr, Benjamin Fuks, David Grellscheid, Olivier Mattelaer, and Thomas Reiter. UFO - The Universal FeynRules Output. *Comput. Phys. Commun.*, 183:1201–1214, 2012. [arXiv:1108.2040](#), [doi:10.1016/j.cpc.2012.01.022](#).
- [49] U. Baur, O. Brein, W. Hollik, C. Schappacher, and D. Wackeroth. Electroweak radiative corrections to neutral current Drell-Yan processes at hadron colliders. *Phys. Rev. D*, 65:033007, 2002. [arXiv:hep-ph/0108274](#), [doi:10.1103/PhysRevD.65.033007](#).

- [50] Glen Cowan, Kyle Cranmer, Eilam Gross, and Ofer Vitells. Asymptotic formulae for likelihood-based tests of new physics. *Eur. Phys. J. C*, 71:1554, 2011. [Erratum: *Eur.Phys.J.C* 73, 2501 (2013)]. [arXiv:1007.1727](#), [doi:10.1140/epjc/s10052-011-1554-0](#).
- [51] Roberto Contino, Adam Falkowski, Florian Goertz, Christophe Grojean, and Francesco Riva. On the Validity of the Effective Field Theory Approach to SM Precision Tests. *JHEP*, 07:144, 2016. [arXiv:1604.06444](#), [doi:10.1007/JHEP07\(2016\)144](#).
- [52] Marco Farina, Giuliano Panico, Duccio Pappadopulo, Joshua T. Ruderman, Riccardo Torre, and Andrea Wulzer. Energy helps accuracy: electroweak precision tests at hadron colliders. *Phys. Lett. B*, 772:210–215, 2017. [arXiv:1609.08157](#), [doi:10.1016/j.physletb.2017.06.043](#).
- [53] Riccardo Torre, Lorenzo Ricci, and Andrea Wulzer. On the W&Y interpretation of high-energy Drell-Yan measurements. *JHEP*, 02:144, 2021. [arXiv:2008.12978](#), [doi:10.1007/JHEP02\(2021\)144](#).
- [54] A. Abada et al. FCC-hh: The Hadron Collider: Future Circular Collider Conceptual Design Report Volume 3. *Eur. Phys. J. ST*, 228(4):755–1107, 2019. [doi:10.1140/epjst/e2019-900087-0](#).
- [55] Giovanni Ossola, Costas G. Papadopoulos, and Roberto Pittau. On the Rational Terms of the one-loop amplitudes. *JHEP*, 05:004, 2008. [arXiv:0802.1876](#), [doi:10.1088/1126-6708/2008/05/004](#).
- [56] Giovanni Ossola, Costas G. Papadopoulos, and Roberto Pittau. Reducing full one-loop amplitudes to scalar integrals at the integrand level. *Nucl. Phys. B*, 763:147–169, 2007. [arXiv:hep-ph/0609007](#), [doi:10.1016/j.nuclphysb.2006.11.012](#).
- [57] P. Mastrolia, G. Ossola, C. G. Papadopoulos, and R. Pittau. Optimizing the Reduction of One-Loop Amplitudes. *JHEP*, 06:030, 2008. [arXiv:0803.3964](#), [doi:10.1088/1126-6708/2008/06/030](#).
- [58] Valentin Hirschi, Rikkert Frederix, Stefano Frixione, Maria Vittoria Garzelli, Fabio Maltoni, and Roberto Pittau. Automation of one-loop QCD corrections. *JHEP*, 05:044, 2011. [arXiv:1103.0621](#), [doi:10.1007/JHEP05\(2011\)044](#).
- [59] Simone Alioli, Radja Boughezal, Emanuele Mereghetti, and Frank Petriello. Novel angular dependence in Drell-Yan lepton production via dimension-8 operators. *Phys. Lett. B*, 809:135703, 2020. [arXiv:2003.11615](#), [doi:10.1016/j.physletb.2020.135703](#).
- [60] Christopher W. Murphy. Dimension-8 operators in the Standard Model Effective Field Theory. *JHEP*, 10:174, 2020. [arXiv:2005.00059](#), [doi:10.1007/JHEP10\(2020\)174](#).
- [61] Hao-Lin Li, Zhe Ren, Jing Shu, Ming-Lei Xiao, Jiang-Hao Yu, and Yu-Hui Zheng. Complete set of dimension-eight operators in the standard model effective field theory. *Phys. Rev. D*, 104(1):015026, 2021. [arXiv:2005.00008](#), [doi:10.1103/PhysRevD.104.015026](#).